Characteristic behaviour of Pebble Bed High Temperature Gas-Cooled Reactors during water ingress events

SN Khoza

Mini-dissertation submitted in partial fulfilment of the requirements for the degree of Master of Science in Nuclear Engineering at the Potchefstroom Campus of the North-West University

Supervisor: Dr D.E. Serfontein

November 2012

ABSTRACT

The effect of water ingress in two pebble bed high temperature gas-cooled reactors i.e. the PBMR-200 $MW_{thermal}$ and the PBMR-400 $MW_{thermal}$ were simulated and compared using the VSOP 99/05 suite of codes.

To investigate the effect of this event on reactivity, power profiles and thermal neutron flux profiles, the addition of partial steam vapour pressures in stages up to 400 bar into the primary circuit for the PBMR-400 and up to 300 bar for the PBMR-200 was simulated for both reactors. During the simulation, three scenarios were simulated, i.e. water ingress into the core only, water ingress into the reflectors only and water ingress into both the core and reflectors. The induced reactivity change effects were compared for these reactors.

An in-depth analysis was also carried out to study the mechanisms that drive the reactivity changes for each reactor caused by water ingress into the fuel core only, the riser tubes in the reflectors only and ingress into both the fuel core and the riser tubes in the reflectors.

The knowledge gained of these mechanisms and effects was used in order to propose design changes aimed at mitigating the reactivity increases, caused by realistic water ingress scenarios. Past results from simulations of water ingress into Pebble Bed Reactors were used to validate and verify the present simulation approach and results. The reactivity increase results for both reactors were in agreement with the German HTR-Modul calculations.

Keywords:

Water ingress, multiplication factor, reactivity increase, Pebble bed high temperature Gas-cooled reactors, PBMR-400, PBMR-200, partial steam vapour pressure, VSOP 99/05

ACKNOWLEDGEMENTS

I would like to sincerely thank my supervisor Dr Dawid Serfontein, especially for his invaluable guidance, patience and always being there on the other end of the phone. I could not have done this without you.

I would also like to thank Mr Frederick Reitsma of PBMR (Pty.) Ltd. for his expertise and guidance, for supplying us with VSOP99/05 models and maps.

Table of Contents

List of figures

List of tables

1 Introduction

Abbreviations

This list contains acronyms and abbreviations used in this document.

Table 1: List of acronyms

Acronym/ Abbreviation	Definition
AVR	Arbeitsgemeinschaftsversuchsreaktor
BISO	Bi-structural Isotropic
DBA	Design Basis Accident
DELDAY	The length of the large burn-up time-steps
ETA (η)	Number of neutrons released in fission per neutron absorbed by a fissile nucleus
HEU	Highly Enriched Uranium
HM	Heavy Metal
HTR	High Temperature Reactor
k_{eff}	Neutron multiplication factor of a finite reactor core
LEU	Low enriched Uranium
LWR	Light Water Reactor
PBMR	Pebble Bed Modular Reactor
RPV	Reactor Pressure Vessel
SSC	Systems, Structures and Components
SG	Steam Generator
TRISO	Tri-structural Isotropic
U	Uranium
VSOP	Very Superior Old Program

1.1 Problem statement

This project is aimed at investigating a noted upset transient of gas cooled reactors, known as water ingress.

The possibility of a water ingress event is a genuine issue to be considered in an indirect layout with Rankine cycle. The presence of water on the tube-side of the steam generators presents a possibility for a penetration of neutron moderating steam into the core which may cause a power excursion for certain core layouts as well as graphite corrosion. Due to the higher pressure, water or steam will flow from the secondary into the primary circuit after the rupture of a steam pipe in the heat exchanger.

This study was launched to understand the characteristic performance of HTR cores in terms of claims of inherent safety, particularly in the PBMR-400 and the PBMR-200 concepts (adopted from the German HTR-Modul). Calculations were performed using the VSOP 99/05 code suite.

1.2 Structure of the report

This report consists of the following chapters:

1. **Introduction**: includes background and motivation of the report, literature survey where the theory on the high temperature gas-cooled reactors and their evolution are discussed.

2. **Computer Models for Core Design and Layout**: the VSOP 99/05 code is introduced and input parameters and methods for the simulation models are discussed.

3. **Results**

4. **Discussions and conclusion**

5. **References**

1.3 Literature survey

1.3.1 Background

The main source of electrical power production in South Africa is coal power generation due to the abundance of fossil fuel. South Africa has the eighth largest coal reserves in the world (Hartnady, 2010: 1), enabling it to produce over 50% of the total electricity on the African continent and at one of the lowest costs in the world. Internationally coal is the most widely used primary fuel accounting for about 36% of the total fuel consumption of the world's electricity production (RSA, 2011: 178). Coal is becoming more expensive to mine because of the increase in demand and depletion of resources. Over and above the escalating price of coal, another challenge has become more apparent since the Copenhagen climate change summit. South Africa needs to take steps to assist in fulfilling its commitments to mitigate climate change as expressed, hence the drive to reduce greenhouse emissions. This means therefore that coal cannot be the answer to challenges that South Africa faces in the medium to long term. A limit of 275 million tons of CO_2 has been imposed on emissions in the South African Integrated Resource Plan: 2010-2030 (DOE, 2011: 6) and this step naturally shifts the base-load alternatives away from coal, in particular pulverised coal, to nuclear and natural gas.

Nuclear energy is among those energy sources producing very low levels of carbon dioxide emissions or other greenhouse emissions from their full life cycle. It is closely comparable with renewables such as wind, solar and hydro in this respect.

The critical difference is that nuclear energy is the only proven option with the capacity to produce greatly expanded supplies of clean electricity on a global scale. Other renewable energy sources may be viable, but their intermittent nature limits the extent to which they can be incorporated into the grid, without destabilising the grid or without requiring expensive methods to stabilise the grid such as pumped storage of backup natural gas turbines. On the other hand nuclear energy is currently the only large-scale cost effective energy source that can reduce CO_2 emissions, while continuing to satisfy the accelerating demand for power with stable and reliable base-load power. In the South African Integrated Resource Plan: 2010-2030 (DOE, 2011: 6) a commitment is proposed to include a nuclear fleet of 9,6 GW; 6,3 GW of coal; 17,8 GW of renewables and 8,9 GW of other generation sources, in addition to all existing and committed power plants including 10 GW committed coal .

After the three major nuclear accidents i.e. Three Mile Island, Chernobyl and Fukushima; nuclear was no longer in the agendas of many countries. Since the South African PBMR project was discontinued in 2010, no design evaluation was performed on it after Fukushima. In order to bring it back to the discussion tables, it must be guaranteed to be safe and economically viable. The adopted solution must present a proper balance between the expectations and user requirements of different stakeholders considering a number of key constraints and risks. These constraints and risks include among others: reducing carbon emissions and new technology uncertainties such as costs, operability, lead time to build, etc.

The Pebble Bed Modular Reactor (PBMR) design is based on the German HTR technology from which South Africa made good progress redesigning it specifically for the Eskom grid, prior to the downsizing of the PBMR (Pty.) Ltd. South Africa could suffer economically if it were to rely solely on energy conservation and other renewable energy options, in order to meet the escalating energy demand, hence the nuclear energy drive.

In Germany the HTR technology started with pebble shaped fuel elements in the AVR reactor from 1967 to 1988 (Moormann, 2008: 8). Despite some safety related issues, the AVR was operated successfully for more than 20 years and showed that an HTR with pebble type fuel can be operated safely. Many types of fuel elements have been tested successfully and important safety experiments have been carried out in this reactor.

The Thorium-HTR, THTR-300 (750MW thermal, 300 MW electrical), was operated from 1985 to 1989 at coolant exit temperatures of 750°C, but for a total of only 1.2 full power years (Moormann, 2008: 9) Despite difficulties during construction and start-up of this plant, the design data of the power plant were fully achieved and the availability of the plant was good. The permanent shutdown of the THTR-300 was caused by some technical problems, which were partly pebble bed-specific and rendered its operation complex and costly (Moormann, 2009: 3).

Gas cooled reactors have been characterised as economically viable and demonstrably safe, based on sustainability and inherent safety features. The ease of waste handling of the PBMR makes it attractive for next generation reactors. The use of helium as coolant and of graphite as structural material allows much higher helium temperatures compared to the systems mentioned above. Therefore, the thermal efficiency is higher.

Helium properties:

- There is no significant neutron interaction at practical pressure levels.
- It is chemically inert.
- Helium is available and the cost will remain only a small fraction of the cost of the reactor operation.
- It cannot be activated and become radioactive and also does not interfere with the neutron moderation process.

An inherently safe reactor is favoured as it plays a major role in cost reduction, as far as the prevention and the consequences of accidents are concerned. The passive safety features of HTRs reduce the need for safety grade backup systems, contributing to the simplicity of the design. There is no possibility of a core melt and helium (the coolant) is chemically and radiologically inert.

The HTR TRISO fuel has a buffer layer of pyrolytic graphite to minimise fission fragments migration and protects the plant from a loss of containment accident, making offsite emergency plans superfluous. The major difference between existing reactor types and HTRs is that, by design, loss of coolant in the PBMR does not lead to fuel failure due to the fuel properties and the passive heat removal.

The three fission barriers for HTRs are formed by the coated particles, the fuel element and the primary circuit. Thus removal of the second barrier does not lead to

gross failure of the fuel fission product retention properties. In the case of PBMR these are provided by the three main coatings of the coated particles. In light water reactors (LWRs), the first barrier is provided by the fuel cladding, the second being the primary system circuit and then the containment acts as a third and final barrier. As a result the integrity of the third barrier as a means to protect the public from an early large dose is of less importance in PBMR than in LWRs.

The peak temperature that can be reached in the core of the reactor during normal operation is designed to be below a temperature that may cause damage to the fuel, which was established as 1600°C (Lohnert, 1990: 259). The reactor is designed not to be hot enough for long enough to cause damage to the fuel. In case of a fault occurring during normal operation, the reactor will shut itself down and should dissipate the decay heat, thereby preventing a core failure or release of fission products to the public and the environment. Therefore no “cliff edge” events are expected in the operation of the PBMR.

The evolution of conceptual designs of the PBMR in South Africa started in the 1990s derived from the 200 $MW_{thermal}$ German HTR-Modul. The first design concept to be investigated was the PBMR 268 $MW_{thermal}$ with an electrical power output into the grid of 110 MW with a core geometry consisting of a central reflector of graphite spheres moving as part of the core with a nominal diameter of 1.75 m. After this, an investigation of a reactor power increase to 400 $MW_{thermal}$ was launched. This provided an opportunity to consider a core with a fixed central reflector of 2 m, a core outer diameter of 3.7 m and an effective nominal height of 11 m (Matzner, 2004: 7).

In 2009, PBMR (Pty.) Ltd. announced the change of focus to be an industrial company, rather than solely an electricity utility, which meant it would also consider process heat applications in addition to creating electricity. Pebble bed reactors are attracting worldwide interest because of their high gas outlet temperatures, allowing applications beyond electricity generation. The focus then changed from designing and building a 400 $MW_{thermal}$ high temperature gas-cooled reactor with a closed Brayton conversion cycle to a more conventional 200 $MW_{thermal}$, gas-cooled and modular, indirect Rankine cycle pebble bed reactor, without a central reflector (McKune, 2010: 2). This design would effectively deliver steam as its main product.

All HTR reactor concepts have some common characteristics independent from the form of the fuel elements (Lohnert, 1990: 263-264):

- Use of full ceramic fuel elements with TRISO coatings, which are capable of retaining all radiologically relevant fission products up to fuel element temperatures of approximately 1600°C allow very high burn-up of fuel,

- Helium as an effective and inert coolant medium. Helium does not significantly influence the neutron balance. In normal operation helium allows very high coolant temperatures. This allows the operation of very efficient steam cycles, gas turbine cycles, combined cycles or the use of nuclear heat for process heat applications

- Full ceramic (graphite) core structures, which allow for the use of high temperatures where graphite is used in core areas with high temperatures (fuel elements, core internals). Temperature-induced failure of this material is impossible at the maximum occurring temperature of 1600°C. The effect of neutron irradiation on the properties of graphite is important in the design and operation of graphite moderated nuclear reactors. Changes of dimensions because of irradiation will be small.

- Reactor cores with low power density, which are very robust and have high heat capacity to make the reactor thermally inert in all operational and control procedures.

- Core designs, which can even tolerate loss of coolant and loss of all active decay heat removal. Self-acting decay heat removal is possible and fuel temperatures stay below admissible values. Therefore, by design, the fission products will remain inside the fuel, even in extreme accidents. The reactor core is designed and laid out in such a manner that a maximum fuel element temperature of 1600°C is not exceeded during any accident.

- Very strong negative temperature reactivity coefficients will contribute to the sound inherent safety characteristic of these reactors, even in hypothetical reactivity accidents concerning the neutron balance. There is a self-acting limitation of nuclear power and fuel temperatures to allowable values. In the case of pebble bed HTRs there is no excess reactivity for burn-up and the contribution of single fuel elements to reactivity is very small.

1.3.1.1 High Temperature Reactor Fuel Elements

Fissile and fertile uranium and or thorium or plutonium is used in the form of coated fuel particles in HTRs. Each fuel element has a diameter of 6 cm and contains approximately 11600 coated particles within the inner graphite matrix. Each of these coated particles shown in Figure 1 below consists of a fuel kernel (uranium dioxide, UO_2) with a diameter of about 0.5 mm, which is coated with a layer of pyrolytic carbon on the outside then silicon carbide (SiC) and the inner pyrolytic carbon to protect the fuel. Around the fuel kernel there is a porous carbon buffer layer. This system allows high operation temperatures under normal conditions (maximum 1350°C) and in accident conditions (maximum 1600°C) without release of unacceptable quantities of fission products (Lohnert: 1990). In different countries various types of fuel elements have been developed and qualified for operation.

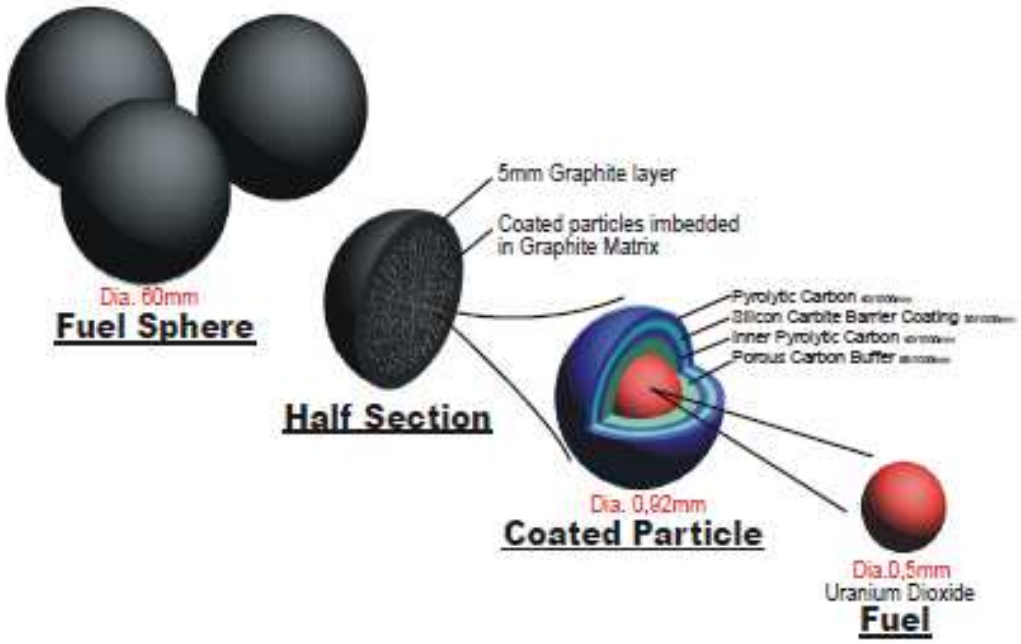

Figure 1: **TRISO coated fuel particle**

1.3.2 Motivation

The South African PBMR-200 designed concept intended to use an indirect Rankine cycle where the primary circuit would be a graphite moderated and helium cooled pebble bed (NECSA: 2012). The helium would then transfer the heat generated in the reactor to the secondary side via a steam generator (SG), heating the feed-water in the tube bundles and thereby producing superheated steam. The disadvantage that comes with using the indirect cycle is the susceptibility to water ingress accidents as steam generator tube breaks have a potential to result in water ingress into the reactor. When a leakage of the steam generator occurs, due to the much

higher pressure of the secondary loop, the water and steam in the steam generator will spray into the primary circuit and flow into the reactor core along with the helium.

An indirect cycle circulates the gaseous coolant in the primary cycle through the heat source removing the heat generated by the source. The hot gas then passes through a heat exchanger transferring the heat to the secondary cycle. This can also be used to generate steam, which is circulated through a traditional steam turbine to generate electricity.

The major advantage of this system is that, in the nuclear industry, the primary cycle consists of a relatively small radioactive cycle thus reducing the risk of nuclear leaks to the environment. As only a blower downstream of the heat exchanger circulates the gas, radioactive build-up on the blades is substantially reduced (Venter: 2009). In more traditional cycles the heat can be produced by any means including coal fires, gas burners etc. The hot gas flowing through the gas turbine can now be kept free from combustion products thereby increasing the life expectancy.

Steam generators are the separation point between the primary and secondary loops. As safety components, they must remain functional under accident conditions and thus a tube bundle leakage needs to be a rare event. This event presents a probability of the water vapour chemically attacking the graphite of the reflector and fuel and forming carbon-oxides and hydrogen. Due to the high steam generator secondary pressure compared to the reactor, prevention of water ingress will be a big consideration.

1.3.3 Reactivity Transient Event

Excess reactivity is the additional reactivity available in the core during operating conditions by the loading of a fuel mixture that is more reactive (less burned) than what is required to keep the reactor critical at full power operating conditions. The excess reactivity is balanced by the insertion of control rods to keep the reactor critical and it can be changed by amending the position of the control rods or adjusting the loading of the fresh fuel into the core.

Reactivity transient events involve reactivity addition but not failure of the helium pressure boundary and so are not expected to add to public or worker dose. During such events the fundamental safety function of containment of radioactivity must be maintained. The fuel temperatures must therefore be kept below a specified limit and

the systems structures and components (SSC) design temperatures must not be exceeded. Above all, after these kinds of incidents, the reactor must be able to be brought to a safe and stable shutdown. One of the major reactivity transient events is reactivity increase due to water ingress and is discussed below.

1.3.3.1 Water Ingress

In general, water ingress into the primary circuit of a high temperature reactor poses a considerable hazard. One of these hazards is that the penetration of neutron moderating steam into the core may cause an intolerable increase in reactivity and thus an intolerable power excursion for certain core layouts. The second hazard is the possibility that steam may be converted by a chemical reaction with the hot graphite structures and the hot graphitic fuel elements into a mixture of H_2 and CO gasses, which might become flammable when mixed with air (Lohnert, 1992; 159).

Because the water pressure in a Rankine cycle is higher than the primary circuit gas pressure, the most likely possibility for moisture ingress is a steam generator leak, which will cause water vapour to enter the core, where it can attack graphite that is at a temperature > 800°C. The oxidation products are CO and H, both of which can form flammable mixtures with air when released from the pressure boundary. As a steam generator leak does not imply a pressure boundary leak, there is little likelihood of releases to the building atmosphere. The accident will be terminated by removing the water vapour or by cooling the core, depending on the result of analysis of the most effective method for various scenarios.

Ingress of water into the core can potentially have a negative back-coupling coefficient, because over-moderation can be achieved by a suited fuel element design. The amount of water, which can ingress into the primary circuit, is limited by a real time cut-off of the steam generator in case of damage and a stop to the feed water supply, as well as the opening of a pressure release valve. The helium blower would immediately cease operation after massive water ingress. Water flows into the core according to the relevant partial pressure. In the case of a negative reactivity coefficient, this will lead to a shut-down of the nuclear chain reaction. However, in the case of a positive reactivity coefficient, which normally applies, this steam ingress will lead to a reactivity and consequently a power and temperature excursion. The over-pressure, due to the addition of the partial pressure of the steam as well as the temperature increase of the helium in the primary circuit, is relieved and decreased

by safety valves, rupture discs (Lohnert, 1992: 166). The consequences of the water ingress event therefore need to be evaluated.

Kugeler et al. (1988: 184) studied the concept of aerosol formation in pebble bed HTRs for a 250 $MW_{thermal}$ reactor and it was established that no reaction gas is produced for reaction temperature below 827°C. The water that intruded into the pebble bed was just vaporised. The dry reaction gas mass flow rose with temperature due to increasing hydrogen and carbon monoxide production. It exceeds the mass flow of the intruded water or steam only when the temperature reaches 1076°C.

As South Africa had previously chosen the direct cycle concepts at different power levels, the studies that were done for the water ingress transient did not include a steam generator leak. Now that the concept is for an indirect steam cycle, the possibility of water ingress due to steam generator tube leak exists.

1.3.4 Related Work

1.3.4.1 AVR

The AVR was the first pebble bed reactor and was operated from 1967 to 1988 in Jülich at Helium outlet temperatures of up to 990°C producing 46 $MW_{thermal}$ (Moormann, 2009: 1). This experimental reactor was developed to demonstrate the technical feasibility of high temperature reactors and the test of many different types of pebble shaped fuel elements. The main design data of the AVR is shown in Table 2 (Moormann, 2008: Table 1) below.

Table 2: Main design parameters of the AVR

Parameter	Unit	
Power	MW_{th}	46
Coolant pressure	bar	10.8
Core height/ diameter	m	2.8/3
Average power density	MW/m^3	2.5
Coolant inlet/ outlet temp	°C	275/ 850-990

This reactor was decommissioned from late 1988 but during its 21 years of operation an incident of water ingress was experienced and this would influence the design of future reactors. In 1978 the moisture content of the coolant circuit was observed to be high and a steam generator leak was suspected (Moormann. 2009: 11).

The steam generator leak remained small and the core temperatures were already low when large amounts of water were present in the core and thus the extent of the graphite/steam reaction was limited.

There were two important lessons learnt from this particular incident (Moormann, 2009: 29) namely:

- The formation rate of burnable gases (CO and H_2) in design basis accidents increase exponentially with temperature and this occurs in steam cycle and in process heat generating concepts.
- Steam generator leaks lead water in the direction of the core and the presence of liquid water in the void volume of a pebble bed may lead to a positive void coefficient of reactivity which may induce reactivity excursion.

1.3.4.2 HTR-Modul

(Lohnert, 1992: 159-176) studied the consequences of water ingress into the primary circuit of an HTR-Modul. Water ingress into the primary circuit was limited by draining the steam generator as soon as humidity was detected. The inherent limitation of the reaction of graphite and water was addressed in two ways. Firstly, the special design features were introduced into the primary and secondary circuit to inherently limit the amount of water that can be carried into the core, once the tube ruptures of the steam generator have happened. The steam generator is slightly below the reactor to avoid direct ingress of water into the core by gravity. Secondly, by choosing a special core design and a special fuel element the core response due to water ingress and thus especially the core temperatures which govern the reaction rate, have been considerably limited.

The HTR-Modul concept is characterised by the fact that all possible reactivity insertions are controlled via negative temperature coefficient without exceeding the limit-temperature of the fuel elements of 1600°C (Lohnert, 1992: 166)

Possible graphite corrosion after water ingress into the primary circuit was one of the major concerns of the HTR safety assessment. In addition, an increase of the core reactivity due to steam ingress into the reactor core was carefully investigated.

When steam ingress occurs, the influx of steam as an additional moderator gives rise to two effects. Firstly, the reactor increases its reactivity since the neutron spectrum

softens, which in turn increases the overall fission cross section. Secondly, due to improved neutron moderation the overall neutron diffusion coefficient decreases, which in turn decreases the overall neutron leakage (Lohnert, 1992: 166). A decrease in neutron leakage however decreases the rod worth of the absorbers in the side reflector, so that in a shutdown or partially shut down core the overall effect of water ingress is the sum of reactivity increase and rod worth decrease.

Two severe hypothetical accidents were studied and the results are shown in Figure 2 below (Lohnert, 1992: Figure 7). The most serious design basis accident (DBA) is postulated to be a double-ended guillotine break of a heating tube of the steam generator. Both ends of the heating tube would release 6 kg/s water and steam into a primary circuit.

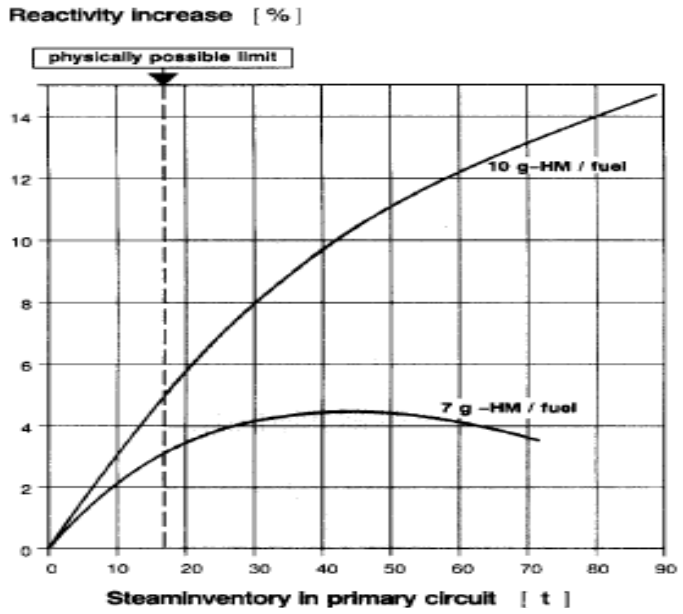

Figure 2: Reactivity increase for the cold, shutdown core.

Figure 2 above shows the results of a reactivity increase study conducted in the HTR-Modul. When an influx of 600 kg of water into the primary circuit at nominal reactor power was set to be the Design Basis Accident (DBA), the power was observed to increase from 200 to 250 MW. If the whole primary circuit would be filled with steam instead of helium at a pressure of 70 bar and a temperature of 270°C, the core reactivity would increase by 2.7%. The shutdown systems would lose approximately 3.3% in rod worth due to the decrease in neutron leakage. The maximum possible excess reactivity increase due to steam ingress would amount to 4.3% (Lohnert, 1992: 175).

1.3.4.3 HTR-10

China started the construction of a 10 MW HTR (HTR-10) in 1995 and the reactor began operation in 2002. The technology of this reactor is based on AVR experiences and follows the principles of the modular HTR-Modul. The 180 cm in diameter and 197 cm in average height reactor core is formed by a pebble bed of about 27 000 spherical fuel elements of 6 cm diameter and a heavy-metal loading of 5g (Wu et. al., 2002: 27-28).
The design average burnup of fuel elements was about 80 000 MWd/t. During the normal operation, the primary loop pressure was 3.0 MPa; the gas outlet temperature is 700°C and the gas inlet temperature is 250°C (Zuying, 2002: 66).

Transient analysis for this reactor was performed assuming the water ingress in the pressure vessel can occur for the accident of the tube rupture of the heat transfer tube of the steam generator (Zuying et al., 1993: 92-96). When the rupture occurs, water and steam in the tubes will ingress into the primary system, and then flow into the reactor core. The steam-helium mixture will be forced into the reactor by the helium blower thereby causing an increase in reactivity which will then lead to graphite oxidation corrosion and a rise in reactor power and fuel temperature. The reactivity effects of water ingress depend on the amount of water that enters the reactor.

Impurities in the helium circuit are H_2, H_2O, CO, CO_2 and CH_4. These substances can corrode the graphite of the fuel elements. The basic chemical reactions induced by water ingress (Kugeler et. al., 1988: 179; Zuying, 2002: 70) include:

$$C + H_2O \rightarrow CO + H_2 \quad (1)$$
$$CO + H_2O \rightarrow CO_2 + H_2 \quad (2)$$
$$C + 2H_2 \rightarrow CH_4 \quad (3)$$
$$C + O_2 \rightarrow CO_2 \quad (4)$$

For water ingress, the effect of oxidation reactions can be ignored because of very low oxygen content in the primary circuit. The transient behaviour of reactivity increase and graphite corrosion of fuel elements and graphite structures were then analysed. This was done assuming one and two steam generator tube ruptures. The results of the two assumed scenarios are summarised in Table 3, below (Zuying et al., 1993: Table 3).

Table 3: Summary of water ingress results due to rupture of SG tubes

Parameter	One tube rupture	Two tube ruptures
Water ingress rate (kg/s)	0.59	1.18
Normalised power	1.7	2.8
Maximum fuel temperature (°C)	866.2 after 46.4s	874.3 after 97s

In (Zuying, 2002: 65-80), the increase of water-steam density in the pebble bed was observed to increase the neutron moderating ability and introduce a positive reactivity. This led to the increase of reactor power and fuel element temperature. The primary pressure increased to the maximum value of 3.5 MPa at about 3 hours. The maximum fuel temperature increased up to 1036.2°C. The maximum water ingress into the primary circuit was 129.9 kg (Zuying, 2002: 79), including the discharge water before isolation and the water from the steam generator and the pipe lines due to the secondary relief system failure after isolation.

1.3.5 Conclusion

The effect of reactivity increase in several designs of the pebble bed gas-cooled reactors has been demonstrated. Accidental water ingress into the core would mean more neutron moderation thereby encouraging a reactivity excursion. By limiting the amount of water that can enter the core, power excursion may be restricted. An important aspect of the study is that by carefully selecting the design features, the water ingress amount can be minimised and the consequences mitigated.

1.4 PBMR-400 MW and PBMR-200 MW descriptions

PBMR has been under development in South Africa since the 1990s, originally with the aim to commission a 400 $MW_{thermal}$ demonstration reactor. Various reactor design concepts evolved from the German HTR-Modul until a revised strategy was adopted by PBMR (Pty.) Ltd in 2009, favouring the development of a 200 $MW_{thermal}$ reactor for both electricity and process heat applications (Thomas, 2011: 2434).

Reactors that were chosen for this study of water ingress are the PBMR-400 and PBMR-200 MW and are therefore briefly described below. The effect of water ingress in these reactors will be studied in chapters to follow.

1.4.1 PBMR-400 MW description

The original design was based on a direct Brayton cycle as this held promise of higher efficiencies. The maximum achievable power levels for the reactor was increased in several design steps in order to reach a set target for installed cost/kW that would be roughly comparable to coal fired power when lifetime costs were evaluated. As a result the design of the reactor core evolved from the original base of 200 $MW_{thermal}$ adopted from the HTR-Modul design to reach 400 $MW_{thermal}$ with an annular core. Because the direct cycle efficiency is very sensitive to gas outlet temperature, a reactor outlet temperature of 900°C was selected with an inlet temperature of less than 500°C (Matzner, 2004: 7). This resulted in the 400 $MW_{thermal}$ (165 $MW_{electrical}$) version with a fixed central reflector in the core. In addition, the power conversion unit was changed from three-shaft vertical to single-shaft horizontal turbine-compressor configuration. The 400 $MW_{thermal}$ core consists of a 2 m diameter central graphite reflector with control rods positioned at radius of about 191 cm, an effective height of 11 m and five fuel flow channels (Matzner, 2004: 7) as illustrated in Figure 3 below.

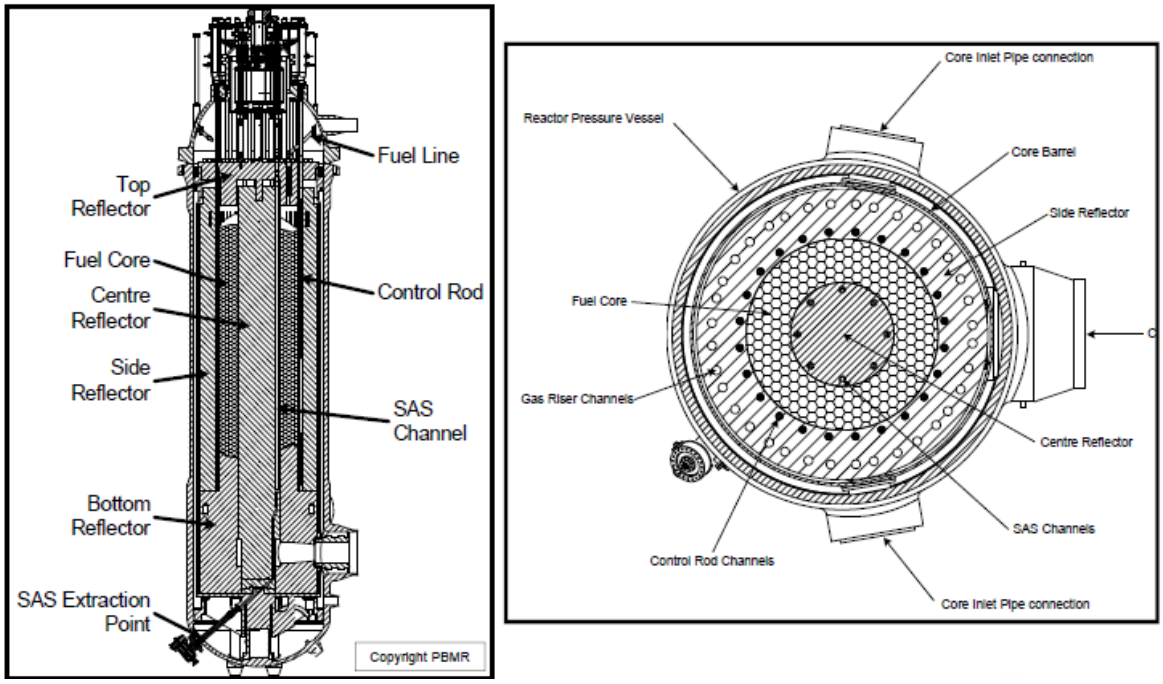

Figure 3: Typical HTGR annular core

Annular cores can be formed by using graphite spheres in the centre or by stacking graphite blocks in the centre. To stay within safety limits the annular core design moved from a dynamic inner reflector to a solid one. The advantage of the dynamic column is that it can easily deal with high levels in fast neutron fluence that is common for the centre part of the core, since it consists of replaceable graphite pebbles that can be circulated together with the fuel pebbles. However, at the boundary of the dynamic inner reflector and the surrounding zone of fuel pebbles a mixing zone exists. In this region the thermal neutron flux peaks and is even higher in the mixing zone than in the fuel zone (NRC: 2010).

1.4.2 PBMR-200 MW Description

In 2009, plans changed to the more conventional steam cycle, and also a much smaller unit, delivering less power i.e. 200 $MW_{thermal}$ (80 $MW_{elecrtical}$). This route was expected to present less technological challenge as standard 'off-the-shelf' steam components could be used thereby reducing timescales and cost and lowering technological risk relative to the 400 $MW_{thermal}$ Brayton cycle PBMR (NECSA: 2012).

The direct cycle design is archived with a view to further progress this design when conditions improve and material development catches up with the demanding conditions of the Brayton cycle. Based on the market research and need to avoid time consuming and costly development work, it was decided that the plant should

consist of smaller modules to better match the market requirements of limited steam and electricity demand as well as high availability but with assurance of supply. (Matzner: 2004).

The new strategy was to pursue the process heat market, for example, desalination and processing tar sands. The thermal output of the reactor would be halved and the helium-driven gas turbine would be replaced by a conventional steam circuit (Thomas, 2011: 2434).

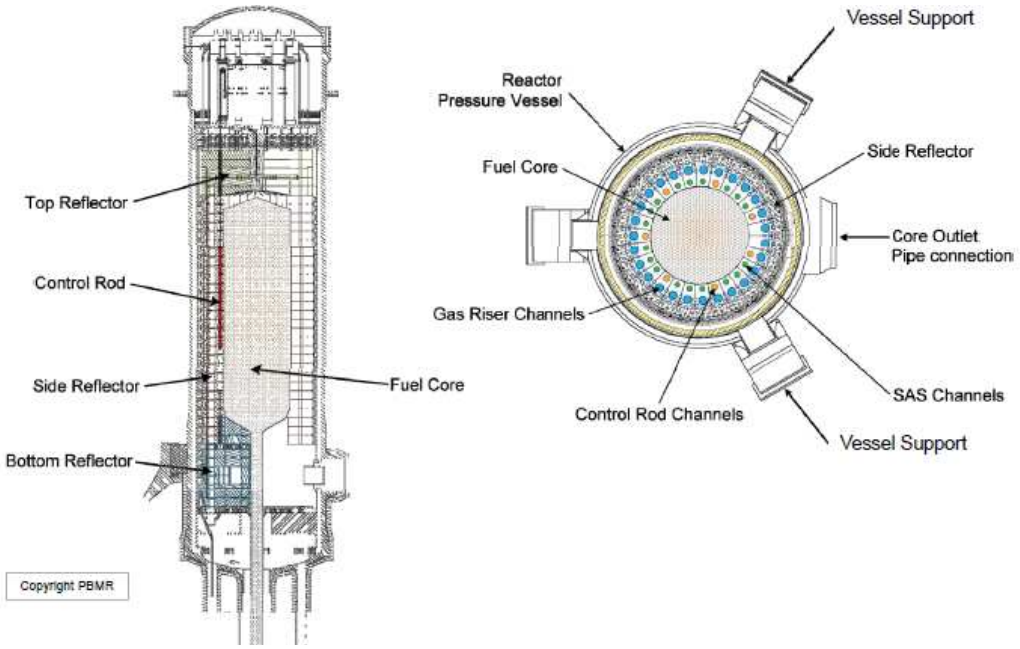

Figure 4: Typical HTGR cylindrical core

1.5 Research aims and objectives

The purpose of the study is to determine the details of the mechanisms and effects of water ingress on the reactivity of the PBMR-400 MW and PBMR-200 MW reactors in order to propose design changes that will mitigate these effects.

Specific research aims will be:

- Study the characteristic behaviour of the reactors in the transient event of water ingress and the impact thereof on k_{eff}, the flux distribution and power profiles for these two reactors.
- Study the difference in the mechanisms and reactivity effects of water ingress into the fuel core only, the riser tubes in the reflectors only and ingress into both the fuel core and the riser tubes in the reflectors.
- Use the knowledge gained of these mechanisms and effects to propose design changes that will mitigate the reactivity increases, caused by realistic water ingress scenarios.
- Use past results from simulations of water ingress into Pebble Bed Reactors to validate and verify the present simulation approach and results.

2 Computer models for core design and layout

This section presents the set of inputs used in this investigation and the 2-D (r,z) simulations that were performed using the VSOP 99/05 analysis code (H.J. Rütten: 2007).

2.1 General description

Fuel element and core design are based on the experience and from a comprehensive library of HTR-Material data. As a first step temperature and geometry dependent resonance integrals are calculated.

Following the program structure, diffusion and burn up calculations are carried out. In these calculations the fission products and the flow behaviour of the pebble bed core are included. Parallel to these neutron physical aspects of burn up the thermo-hydraulic behaviour, i.e. heat production, coolant flow and temperature distribution, of the helium coolant gas, fuel elements and internal reactor structures, such as the reflectors, core barrel conditioning system and pressure vessel, are calculated.

The temporal evolution of the spatial dependence of neutron-flux, the core power density, temperature, neutron spectrum and fuel nuclide composition is recalculated iteratively in sequential cycles until convergence is achieved. As a result of this total calculation process, a restart library of data sets for the total core is available for further analysis by restart runs and additional computer codes.

Table 4: Summary of equilibrium core parameters

Description	Units	PBMR-400 (Reitsma: 2011)	PBMR-200 (Lohnert: 1990)
Core thermal power	MW	400	200
Core diameter (inner/outer)	m	2.0/3.7	3
Core height (average)	m	11.0	9.4
Typical core geometry	-	Annular	Cylindrical
Fuel sphere diameter	cm	6	6
Outer radius of the fuel free zone	cm	2.5	2.5
Helium coolant temperatures (inlet/outlet)	°C	500/900	250/700
Primary system pressure	bar	90	70
Pebble heavy metal loading	g	9	7
^{235}U enrichment	wt%	9.6	7.8
Average residence time in core	Days	~ 930	~ 923
Average discharge burn-up	MWd/t	91 450	80 000
Number of fuel spheres	-	~ 452 000	~360 000
Average number of fresh fuel spheres to be loaded per day	-	~ 486	~ 320
Average number of fuel spheres re-circulated per day	-	~ 2 936	~ 2000

2.1.1 Multiplication factor

The multiplication factor, denoted by k-effective (k_{eff}), is defined as the ratio of the number of fissions in one generation divided by the number of fissions in the preceding generation. When k_{eff} equals one, the chain reaction proceeds at a constant rate, energy is released at a steady level and the reactor is said to be critical (Lamarsh and Baratta, 2001: 117-119). To increase the power produced by a reactor, the k_{eff} value must be adjusted to be greater than one and once the desired power level has been reached, the value of k_{eff} must be adjusted back to one. K_{eff} is a measure of the ability of a reactor to regenerate neutrons by the fission process and is therefore commonly used as a measure of criticality safety.

2.1.2 Reactivity

When steam ingress into the fuel core occurs, the influx of steam acts as an additional moderator. Since mass of an ^{1}H nucleus is almost identical to that of a neutron, the ^{1}H in the steam decreases the energy of the neutron much more per collision (i.e. its lethargy is much higher) than for the ^{12}C in the fuel and reflectors. Neutron collision is defined in terms of energy, lethargy u as:

$$u = \ln \frac{E_0}{E}$$

where, E_0 is the maximum energy that a neutron might have in a nuclear reactor (Lamarsh and Baratta, 2001: 71). At high energies, the neutron's lethargy is low and as it slows down its lethargy increases. A neutron can scatter from any lethargy to any greater lethargy in a single collision with hydrogen, i.e. it is possible for a neutron to lose up to 100% of its energy in a single collision with a ^{1}H nucleus. For moderators other than hydrogen, it is not possible for a neutron to lose all of its energy in a single collision.

This increase in neutron moderation increases the reactivity of the reactor since the neutron spectrum softens, which in turn increases the average microscopic fission cross section in the thermal energy region. Due to improved neutron moderation, the number of neutrons captured in the radiative capture resonances of ^{238}U in the fuel kernels decreases and thus the resonance escape probability increases. These two factors cause a substantial increase in k_{eff}. However microscopic cross sections for radiative capture (σ_γ) in ^{1}H in the steam are much higher than in the natural carbon (^{Nat}C) in the graphite as is shown in Figure 5 below. This increase in captures in the fuel core partially offsets the increase in k_{eff} described above.

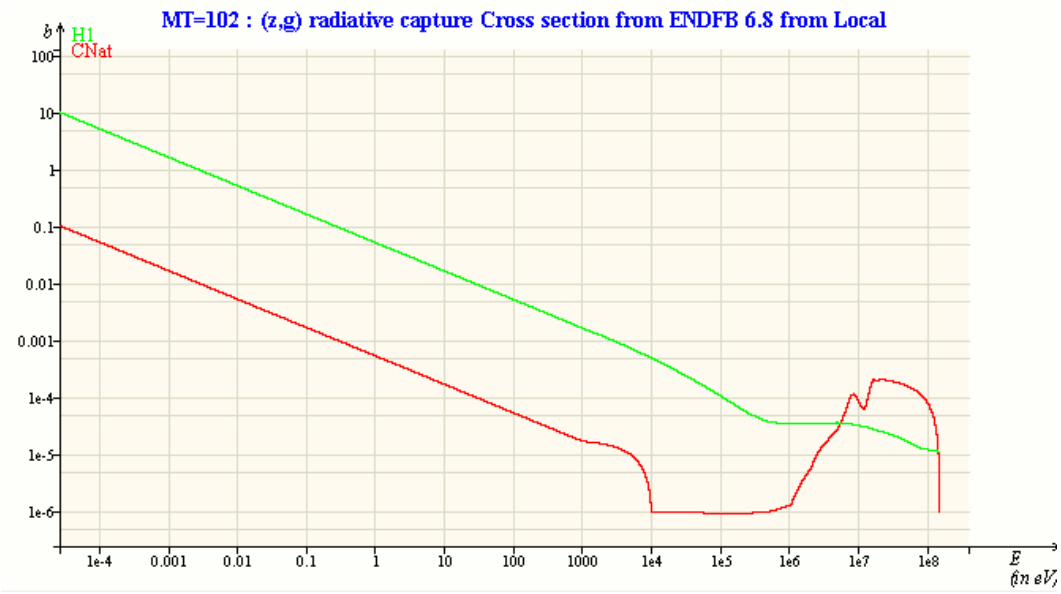

Figure 5: Radiative capture cross section of ^{1}H and ^{nat}C

When the steam ingress occurs into the reflectors, increases in neutron capture become more pronounced: the high values of σ_γ for ^{1}H occur at the thermal energies. Therefore, since the neutrons in the reflectors are much more thermalised than in the fuel, the steam in the reflectors is significantly more effective at capturing neutrons than the steam in the fuel. Furthermore in the thermal energy region σ_γ for ^{Nat}C increases substantially with decreasing energy. Therefore the increased moderation supplied by the ingressing water will also increase the captures in the graphite. Since the VSOP codes assign all captures in the reflectors to the category of leaked neutrons, water ingress into the reflectors will substantially increase the leakage and thus decrease k_{eff}. The captures in the epithermal resonances of ^{238}U, on the other hand, occur in the fuel only. Therefore, while increased moderation due to water ingress into the fuel will decrease these captures and will thus increase k_{eff}, no such reduction in captures will occur for water ingress into the reflectors. The combination of these mechanisms predict opposing reactivity increases for water ingress into the fuel core and reactivity decreases for ingress into the reflectors.

2.1.2.1 Fissionable materials cross sections

When a neutron interacts with a fissile nucleus (^{235}U, ^{239}Pu and ^{241}Pu) at low energies, the phenomenon that results is either radiative capture, elastic scattering or fission. The fission cross section, σ_f, is a measure of the probability that a neutron and a nucleus interact to form a compound nucleus which then undergoes fission.

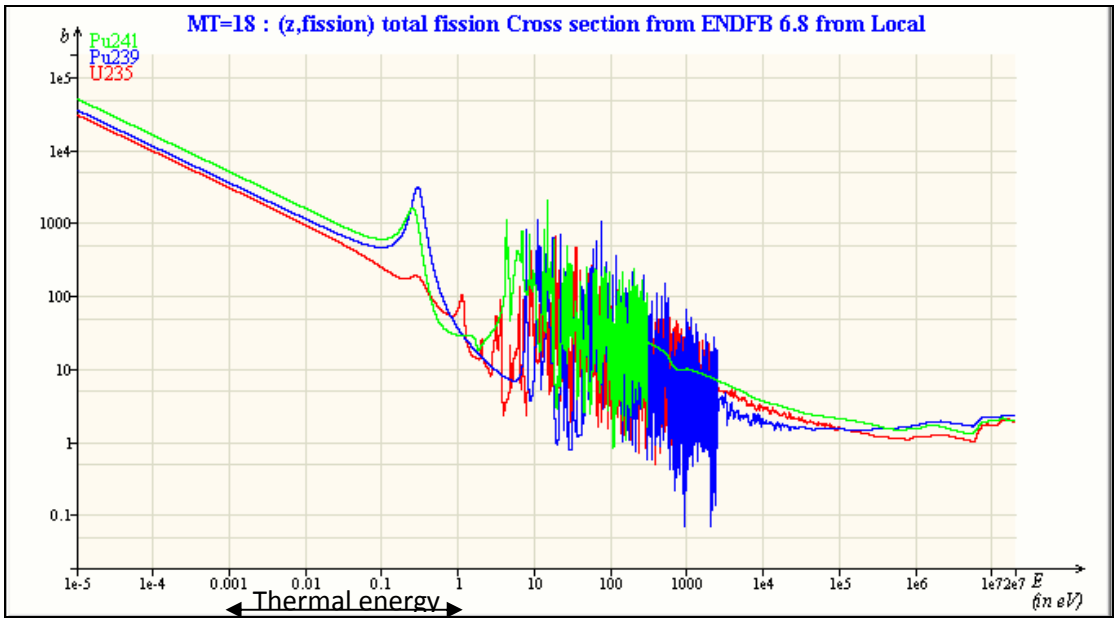

Figure 6: Fission cross sections for fissile material

It can be seen from Figure 6 above that the fission cross sections are largest in the thermal energy region, i.e. E < 1 eV. The thermal fission cross section for ^{239}Pu is larger than that for ^{235}U or ^{241}Pu.

A fertile material such as ^{238}U is one that will capture a neutron, and transmute by radioactive decay into a fissile material. Fertile isotopes may also undergo fission directly, but only if impacted by a high energy neutron. Fission and radiative capture cross sections for ^{238}U are shown in Figure 7 below. It can be observed that the fission cross section is insignificant below about 1 MeV except for resonances, above which it is about 1 barn. Radiative capture cross section is substantially higher especially at resonances and decreases above 1 MeV.

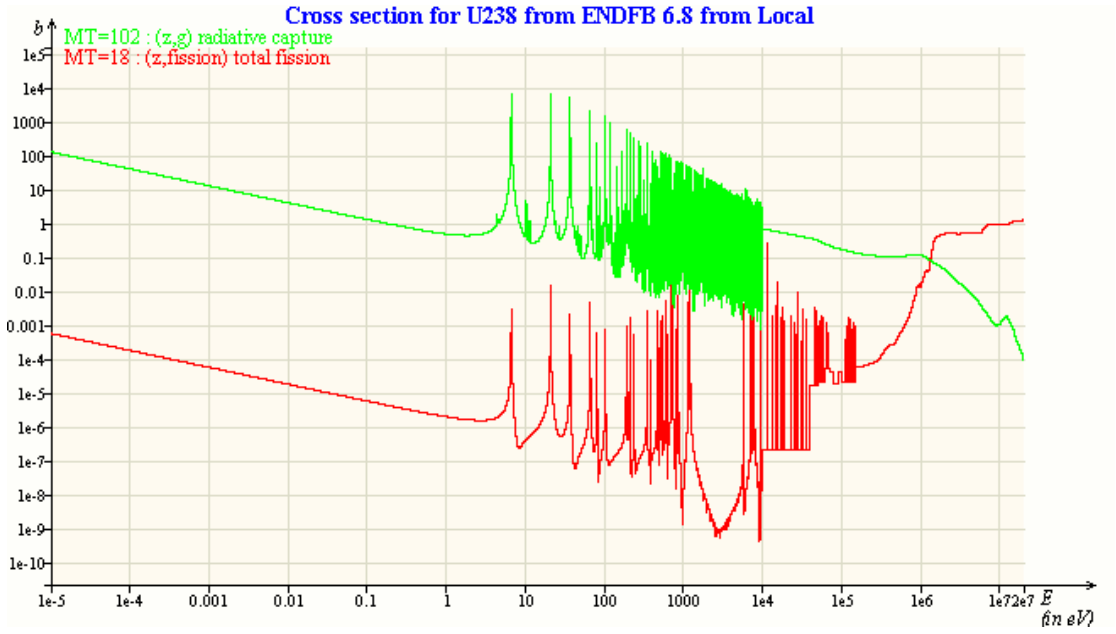

Figure 7: Fission and radiative capture cross sections for ^{238}U

2.1.3 Thermal flux

In thermal reactors, fissions are largely caused by thermal neutrons diffusing into the fuel from the moderator. The thermal neutrons are generated from fast fission neutrons which escape capture in the fuel and are slowed down in the moderator as explained in section 2.1.2 above. In reflected cores, thermal flux is found to rise near the core-reflector interface and peak in the reflectors due to thermalisation of fast neutrons that escape the core and accumulate in the reflector. The flux will show a trough in the core and a hump in the adjacent reactor. This dip can be attributed to thermal neutrons being strongly absorbed in the fuel, due to the high microscopic fission cross sections of the fissile fuel nuclides.

2.1.4 Primary relief system

In the German HTR-Modul, the pressure relief valves in the primary circuit, which discharge into the reactor building, respond at approximately 70 bar. The safety valve closes again once the primary pressure has reached its design value of 60 bar. Should the first valve not open then the second train of the relief system will be actuated at an overpressure of 72 bar yielding a discharge area of 23 cm^2, which allows approximately 10 kg/s of primary helium to be discharged into the reactor building (Lohnert, 1990: 163).

2.1.5 Approximations and simplifications

The models were established based on some approximations and simplifications as described below:

- Both models are created in 2-D configuration, as a result some of the 3-D and other neutronic effects are simplified.
- The control rod channel is neutronically important since it is close to the core and was correctly modelled,
- As described in section 2.1.4 above, pressures above 70 bar would render pressure relief valves open to release helium and water out of the core. During the analysis, it was assumed that the pressure relief system was not available and therefore partial steam vapour pressures of up to 400 bar were simulated.

2.2 PBMR-400 MW core design

2.2.1 Steady state model

2.2.1.1 Core model

The 400 MW core model comprises of an annular core of 3.7 m and a fixed central graphite reflector of 2 m in diameter, an effective cylindrical core height of 11 m (Reitsma, 2012: 19). The PBMR-400 core model used in this study is shown in Figure 8 below and was developed for (Serfontein, 2011: Figure 11). The system pressure is 90 bar. For practical calculations the core is divided into batches which are all filled with the fuel material, while the outer lying regions of the reactor comprise of the reflector material, vessel material, void regions, etc. According to this discrete mesh pattern, the simulation will provide batchwise data for the fuel shuffling, cost evaluation and the decay heat production parameters during steady state and quasi steady state transients.

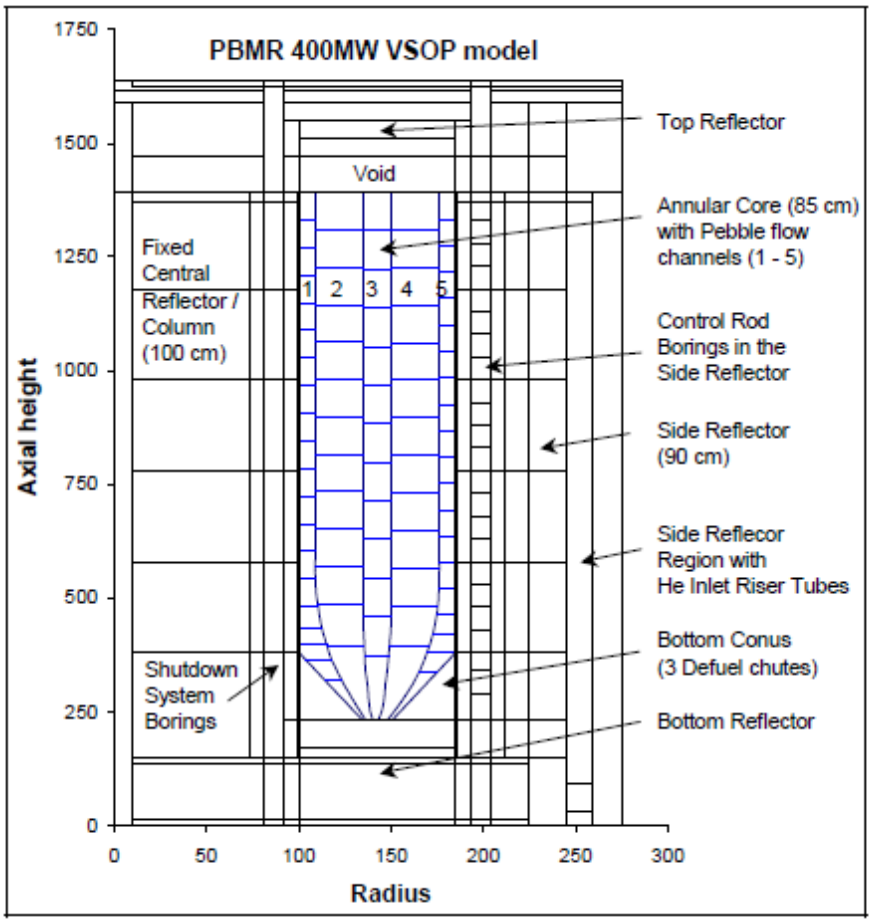

Figure 8: PRMR-400 VSOP core model

2.2.1.1.1 Fuel management

Heavy metal (uranium) loading is 9g per fuel-sphere with a ^{235}U enrichment of 9.6 wt%. Each fuel sphere is 6 cm in diameter and the outer radius of the fuel zone is 2.5 cm. Each of the UO_2 fuel kernels has a density of 10.41 g/cm^3. The fuel elements are passed six times through the core before they reach their target burn-up. Online refuelling and multi-pass ensure low excess reactivity, a flatter burn-up profile with an increased number of passes and eliminate the need for shutdown to re-fuel. There are five fuel flow channels inside the core and 24 axial regions, i.e. layers, in the two outer fuel flow channels and 18 in the three inner channels. Each region consists of six fuel batches, with each batch representing a different recirculation pass of the fuel. A tiny 7th batch was added to account for round-off errors in the calculation of the volumes of these regions.

2.2.1.1.2 Burn-up time steps

Two large burn-up time steps were used in one burn-up cycle with one large time step containing ten small time steps. These time steps represent the time between possible diffusion and/or spectrum calculations. The length of the large burn-up time steps, denoted by DELDAY in the VSOP 99/05 manual (H.J. Rütten, 2007), was redefined in iterations in order to get k_{eff} close to unity, using restart runs. Once k_{eff} converged to unity, the resulting time-step was used in the steady state calculation. The water ingress event was then simulated.

2.2.2 Water ingress model

In the water ingress simulation, all the fuel with gas flow regions, gas-flow pipes (riser tubes) and voids above the fuel core were identified from the properties of the THERMIX-regions, i.e. the input model for the thermo-hydraulics simulations. These areas are marked in blue in Figure 9 below. The one-to-one correspondence with the map for the VSOP-Batches was then used to identify the corresponding VSOP-Batch numbers for the neutronics simulations as shown in Figure 10 below. These Batch numbers were then used to specify the region into which water ingress takes place for the neutronics simulations. This was done by adding the Batch numbers to the water-ingress cards (R20A for water ingress into the core and R20B for the reflectors batches) in the restart file. The reactor state was frozen in order to prepare for water ingress. This was done by reducing the number of large burn-up time steps per burn-up cycle (variable JNSTOP in card R9) from two to one. This was done in order to freeze k_{eff} in the middle of the last steady state burn-up cycle. This freezing was

completed by stopping the fuel shuffling and reducing the length of the large burn-up time steps to virtually zero. The water ingress transient was then initiated.

To simulate this event, water (steam) was added into the core and chosen reflector batches as per the mapping process described above. The amount of water ingress was specified by specifying successive increases in the partial vapour pressure of steam in the respective regions. The resulting partial steam vapour pressures were 30, 60, 100, 200, 300 and 400 bar.

The void fraction of pebble bed core is 0.61 and the corresponding porosity 0.39 (Mulder: 2010). The mass equivalent of these partial steam vapour pressures were then calculated with the core volumes of 83.73 m^3 for the PBMR-400 and 66.16 m^3 for the PBMR-200 and are shown in Table 5 below.

Table 5: Mass equivalent of partial steam vapour pressures used in the simulations

Partial Steam Vapour Pressure (bar)	Amount of water added (kg)	
	PBMR-200	PBMR-400
30	217	275
60	434	549
100	723	915
200	1447	1831
300	2170	2746
400	2893	3661

The following three scenarios were studied:

1) Water ingress into the fuel core.
2) Water ingress into the reflectors.
3) Water ingress into both the core and reflectors.

At specified time intervals, operational data including neutron flux and power distribution was stored for further investigation. The results of the study are shown in Chapter 3.

12	12	12	12	12	12	12	12	12	12	12	12	12	12	12	12	12	12	12	12	12	12	12	12	12
11	11	11	11	11	11	11	11	11	11	11	11	11	11	11	11	11	11	11	11	11	11	11	26	25
10	10	10	10	10	10	10	10	10	10	10	10	10	10	10	10	10	10	10	10	10	10	10	24	25
5	5	5	5	3	3	3	3	3	3	3	3	3	4	4	4	4	4	4	20	21	22	23	24	25
5	5	5	5	2	2	2	2	2	2	2	2	2	4	4	4	4	4	4	20	21	22	23	24	25
5	5	5	5	1	1	1	1	1	1	1	1	1	15	15	15	15	15	4	20	21	22	23	24	25
5	5	5	5	1	1	1	1	1	1	1	1	1	4	4	4	4	14	4	20	21	22	23	24	25
5	5	5	5	1	1	1	1	1	1	1	1	1	4	4	4	4	14	4	20	21	22	23	24	25
5	5	5	5	1	1	1	1	1	1	1	1	1	4	4	4	4	14	4	20	21	22	23	24	25
5	5	5	5	1	1	1	1	1	1	1	1	1	4	4	4	4	14	4	20	21	22	23	24	25
5	5	5	5	1	1	1	1	1	1	1	1	1	4	4	4	4	14	4	20	21	22	23	24	25
5	5	5	5	1	1	1	1	1	1	1	1	1	4	4	4	4	14	4	20	21	22	23	24	25
5	5	5	5	1	1	1	1	1	1	1	1	1	4	4	4	4	14	4	20	21	22	23	24	25
5	5	5	5	1	1	1	1	1	1	1	1	1	4	4	4	4	14	4	20	21	22	23	24	25
5	5	5	5	1	1	1	1	1	1	1	1	1	4	4	4	4	14	4	20	21	22	23	24	25
5	5	5	5	1	1	1	1	1	1	1	1	1	4	4	4	4	14	4	20	21	22	23	24	25
5	5	5	5	1	1	1	1	1	1	1	1	1	4	4	4	4	14	4	20	21	22	23	24	25
5	5	5	5	1	1	1	1	1	1	1	1	1	4	4	4	4	14	4	20	21	22	23	24	25
5	5	5	5	1	1	1	1	1	1	1	1	1	4	4	4	4	14	4	20	21	22	23	24	25
5	5	5	5	1	1	1	1	1	1	1	1	1	4	4	4	4	14	4	20	21	22	23	24	25
5	5	5	5	1	1	1	1	1	1	1	1	1	4	4	4	4	14	4	20	21	22	23	24	25
5	5	5	5	1	1	1	1	1	1	1	1	1	4	4	4	4	14	4	20	21	22	23	24	25
5	5	5	5	1	1	1	1	1	1	1	1	1	4	4	4	4	14	4	20	21	22	23	24	25
5	5	5	5	1	1	1	1	1	1	1	1	1	4	4	4	4	14	4	20	21	22	23	24	25
5	5	5	5	1	1	1	1	1	1	1	1	1	4	4	4	4	14	4	20	21	22	23	24	25
5	5	5	5	16	1	1	1	1	1	1	1	16	4	4	4	4	14	4	20	21	22	23	24	25
5	5	5	5	16	16	1	1	1	1	1	16	16	4	4	4	4	14	4	20	21	22	23	24	25
5	5	5	5	16	16	16	1	1	1	16	16	16	4	4	4	4	14	4	20	21	22	23	24	25
5	5	5	5	16	16	16	16	16	16	16	16	16	4	4	4	4	14	4	20	21	22	23	24	25
5	5	5	5	17	17	17	17	17	17	17	17	17	4	4	4	4	13	4	20	21	22	23	24	25
5	5	5	5	6	6	6	6	18	6	6	6	6	4	4	4	4	4	4	20	21	22	23	24	25
5	5	5	5	6	6	6	6	19	6	6	6	6	4	4	4	4	4	4	20	21	22	23	24	25
5	5	5	5	6	6	6	6	5	6	6	6	6	4	4	4	4	4	4	20	21	22	23	24	25
7	7	7	7	7	7	7	7	7	7	7	7	7	7	7	7	7	7	7	7	7	7	7	24	25
8	8	8	8	8	8	8	8	8	8	8	8	8	8	8	8	8	8	8	8	8	8	8	26	25
9	9	9	9	9	9	9	9	9	9	9	9	9	9	9	9	9	9	9	9	9	9	9	9	9

Figure 9: THERMIX regions for the PBMR-400 in cards TX13

778	778	778	778	778	778	778	778	778	778	778	778	778	778	732	779	779	779	779	779	780	811	811
805	718	792	717	782	782	782	782	782	782	782	782	782	782	732	783	783	783	783	759	780	810	811
805	718	792	717	771	771	771	771	771	771	771	771	771	771	732	770	770	770	770	759	780	810	811
805	718	792	717	719	719	719	719	719	719	719	719	719	727	732	744	749	749	749	759	780	810	811
805	718	793	717	720	720	720	720	720	720	720	720	720	727	733	754	754	754	749	759	780	810	811
806	775	794	804	0	0	0	0	0	0	0	0	0	728	734	745	750	755	812	760	780	810	811
806	775	794	804	0	0	0	0	0	0	0	0	0	728	734	745	750	755	812	760	780	810	811
806	775	794	804	0	0	0	0	0	0	0	0	0	728	734	745	750	755	812	760	780	810	811
806	775	795	804	0	0	0	0	0	0	0	0	0	728	735	745	750	755	812	760	780	810	811
806	775	795	804	0	0	0	0	0	0	0	0	0	728	735	745	750	755	812	760	780	810	811
806	775	796	804	0	0	0	0	0	0	0	0	0	728	736	745	750	755	812	760	780	810	811
806	775	796	804	0	0	0	0	0	0	0	0	0	728	736	745	750	755	812	760	780	810	811
807	776	797	772	0	0	0	0	0	0	0	0	0	729	737	746	751	756	813	761	780	810	811
807	776	797	772	0	0	0	0	0	0	0	0	0	729	737	746	751	756	813	761	780	810	811
807	776	798	772	0	0	0	0	0	0	0	0	0	729	738	746	751	756	813	761	780	810	811
807	776	798	772	0	0	0	0	0	0	0	0	0	729	738	746	751	756	813	761	780	810	811
807	776	799	772	0	0	0	0	0	0	0	0	0	729	739	746	751	756	813	761	780	810	811
807	776	799	772	0	0	0	0	0	0	0	0	0	729	739	746	751	756	813	761	780	810	811
807	776	799	772	0	0	0	0	0	0	0	0	0	729	739	746	751	756	813	761	780	810	811
807	776	799	772	0	0	0	0	0	0	0	0	0	729	739	746	751	756	813	761	780	810	811
808	777	800	773	0	0	0	0	0	0	0	0	0	730	740	747	752	757	814	762	780	810	811
808	777	800	773	0	0	0	0	0	0	0	0	0	730	740	747	752	757	814	762	780	810	811
808	777	801	773	0	0	0	0	0	0	0	0	0	730	741	747	752	757	814	762	780	810	811
808	777	801	773	0	0	0	0	0	0	0	0	0	730	741	747	752	757	814	762	780	810	811
808	777	802	773	0	0	0	0	0	0	0	0	0	730	742	747	752	757	814	762	780	810	811
808	777	802	773	0	0	0	0	0	0	0	0	0	730	742	747	752	757	814	762	780	810	811
808	777	803	774	0	0	0	0	0	0	0	0	0	731	743	748	753	758	815	763	780	810	811
808	777	803	774	0	0	0	0	0	0	0	0	0	731	743	748	753	758	815	763	780	810	811
809	774	774	774	722	726	726	726	721	726	726	726	723	731	731	748	753	758	815	763	780	810	811
809	788	788	788	784	726	726	726	721	726	726	726	785	786	786	786	786	787	786	763	780	810	811
809	774	774	774	724	726	726	726	721	726	726	726	725	764	764	764	765	768	765	763	780	810	811
809	789	789	789	724	726	726	726	721	726	726	726	725	790	790	790	791	791	791	763	780	810	811
809	774	774	774	724	726	726	726	721	726	726	726	725	764	764	764	765	765	765	763	780	810	811
809	774	774	774	769	769	769	769	769	769	769	769	769	766	766	766	766	766	766	763	780	810	811
809	774	774	774	767	767	767	767	767	767	767	767	767	766	766	766	766	766	766	763	780	810	811
781	781	781	781	781	781	781	781	781	781	781	781	781	781	781	781	781	781	781	781	780	811	811

Figure 10: Final ID. Numbers of PBMR-400 VSOP-Batches

2.2.2.1 Neutron flux distribution

Printouts were requested also for the thermal neutron flux and the results are presented and analysed in Chapter 3. To illustrate the effect of water ingress on neutron thermalisation, the results for both fast and thermal energy group are shown. The radial distance at which the maximum thermal neutron flux occurred was located and the flux at this distance was compared before and after water ingress for the cases of reflector ingress only, core only and both core and reflector .

2.2.2.2 Power density distribution

Snapshots of the power density distribution, at different stages of the water ingress event were taken from VSOP. The first one was done before the water ingress and the second one at the value of partial steam vapour pressure that would give the maximum reactivity increase. The printouts were therefore requested at 0 and at 300 bar partial steam vapour pressure for both the PBMR-400 and PBMR-200 reactors. These results are shown and analysed in Chapter 3.

2.3 PBMR-200 MW CORE DESIGN

2.3.1 Steady state model

2.3.1.1 Core model

The PBMR-200 core model has a cylindrical core of 9.43 m in height. The primary system pressure is 70 bar. The PBMR-200 core model shown in Figure 11 below as used in this study was developed for (Geringer 2010: Figure 9).

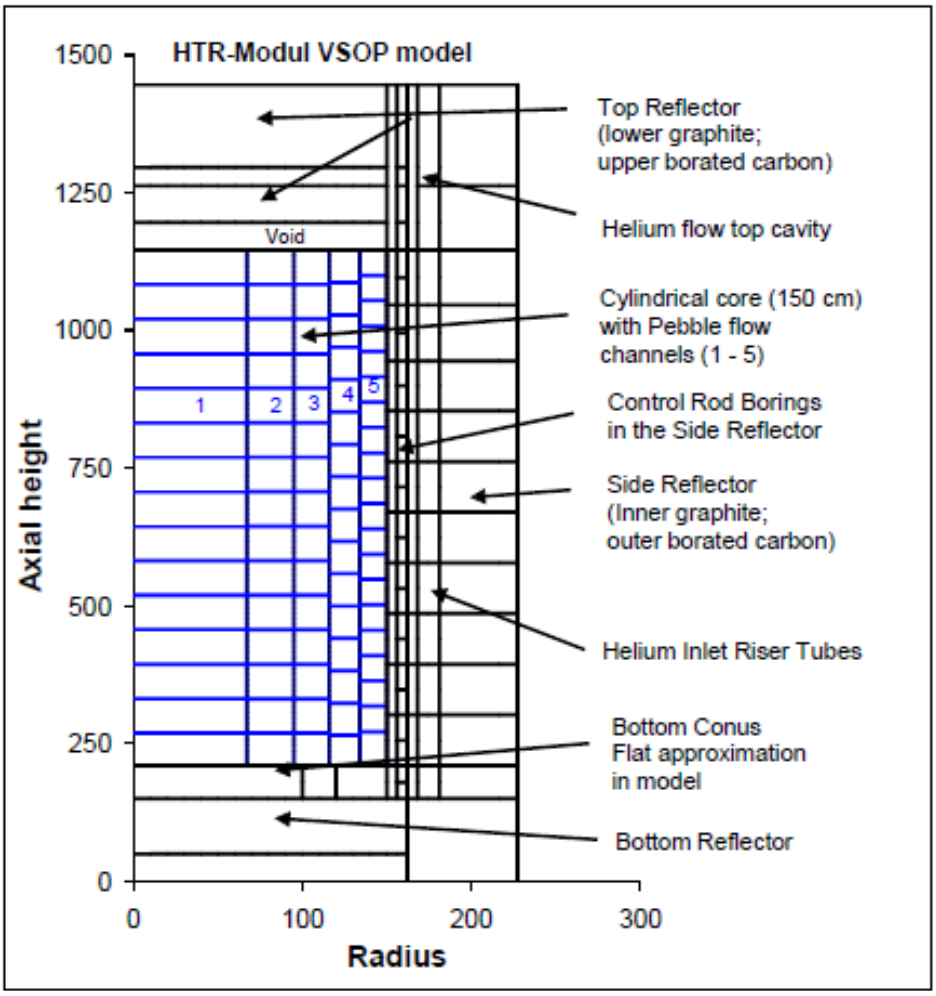

Figure 11: PBMR-200 VSOP core model

2.3.1.2 Fuel management

Heavy metal (uranium) loading is 7g per fuel-sphere with a ^{235}U enrichment of 8 wt% (Venter: 2009). The fuel dimensions are the same as for the PBMR-400 mentioned above. Each of the fuel kernels has a density of 10.41 g/cm^3.

2.3.2 Water ingress model

Similar to the PBMR-400 water ingress model described in section 2.2.2 above, water ingress was simulated for the cases of reflector ingress only, core only and both core and reflector. Addition of partial steam vapour pressures of 30, 60, 100, 200 and 300 bar were studied. The THERMIX-regions and VSOP-Batches mapping are shown in Figure 12 and Figure 13 below. The results of the study are shown in Chapter 3.

12	12	12	12	12	12	12	12	12	12	12	12	12	12	12	12	12	12	12	12	12	12	12	12	12	12	12	12	17
25	25	25	25	25	25	25	25	25	25	25	25	25	25	25	25	25	25	25	25	25	25	25	25	25	25	25	4	23	15	16	17
14	14	14	14	14	14	14	14	14	14	14	14	14	14	14	14	14	14	14	14	14	14	14	14	14	14	14	14	23	15	16	17
24	24	24	24	24	24	24	24	24	24	24	24	24	24	24	24	24	24	24	24	24	24	24	24	24	24	24	22	14	23	15	16	17
7	7	7	7	7	7	7	7	7	7	7	7	7	7	7	7	7	7	7	7	7	7	7	4	24	24	22	14	23	15	16	17
3	3	3	3	3	3	3	3	3	3	3	3	3	3	3	4	4	18	4	20	4	6	4	24	24	22	14	23	15	16	17
2	2	2	2	2	2	2	2	2	2	2	2	2	2	2	4	4	18	4	20	4	6	4	24	24	22	14	23	15	16	17
1	1	1	1	1	1	1	1	1	1	1	1	1	1	1	4	4	18	4	20	4	6	4	24	24	22	14	23	15	16	17
1	1	1	1	1	1	1	1	1	1	1	1	1	1	1	4	4	18	4	20	4	6	4	24	24	22	14	23	15	16	17
1	1	1	1	1	1	1	1	1	1	1	1	1	1	1	4	4	18	4	20	4	6	4	24	24	22	14	23	15	16	17
1	1	1	1	1	1	1	1	1	1	1	1	1	1	1	4	4	18	4	20	4	6	4	24	24	22	14	23	15	16	17
1	1	1	1	1	1	1	1	1	1	1	1	1	1	1	4	4	18	4	20	4	6	4	24	24	22	14	23	15	16	17
1	1	1	1	1	1	1	1	1	1	1	1	1	1	1	4	4	18	4	20	4	6	4	24	24	22	14	23	15	16	17
1	1	1	1	1	1	1	1	1	1	1	1	1	1	1	4	4	18	4	20	4	6	4	24	24	22	14	23	15	16	17
1	1	1	1	1	1	1	1	1	1	1	1	1	1	1	4	4	18	4	20	4	6	4	24	24	22	14	23	15	16	17
1	1	1	1	1	1	1	1	1	1	1	1	1	1	1	4	4	18	4	20	4	6	4	24	24	22	14	23	15	16	17
1	1	1	1	1	1	1	1	1	1	1	1	1	1	1	4	4	18	4	20	4	6	4	24	24	22	14	23	15	16	17
1	1	1	1	1	1	1	1	1	1	1	1	1	1	1	4	4	18	4	20	4	6	4	24	24	22	14	23	15	16	17
1	1	1	1	1	1	1	1	1	1	1	1	1	1	1	4	4	18	4	20	4	6	4	24	24	22	14	23	15	16	17
1	1	1	1	1	1	1	1	1	1	1	1	1	1	1	4	4	18	4	20	4	6	4	24	24	22	14	23	15	16	17
1	1	1	1	1	1	1	1	1	1	1	1	1	1	1	4	4	18	4	20	4	6	4	24	24	22	14	23	15	16	17
1	1	1	1	1	1	1	1	1	1	1	1	1	1	1	4	4	18	4	20	4	6	4	24	24	22	14	23	15	16	17
1	1	1	1	1	1	1	1	1	1	1	1	1	1	1	4	4	18	4	20	4	6	4	24	24	22	14	23	15	16	17
1	1	1	1	1	1	1	1	1	1	1	1	1	1	1	4	4	18	4	20	4	6	4	24	24	22	14	23	15	16	17
1	1	1	1	1	1	1	1	1	1	1	1	1	1	1	4	4	18	4	20	4	6	4	24	24	22	14	23	15	16	17
1	1	1	1	1	1	1	1	1	1	1	1	1	1	1	4	4	18	4	20	4	6	4	24	24	22	14	23	15	16	17
8	8	8	8	8	8	8	8	8	8	8	8	8	8	8	4	4	18	4	20	4	6	4	24	24	22	14	23	15	16	17
8	8	8	8	8	8	8	8	8	8	8	8	8	8	8	4	4	29	4	21	4	6	4	24	24	22	14	23	15	16	17
9	9	9	9	9	9	9	9	9	9	9	9	9	9	9	9	9	9	4	4	4	6	4	24	24	22	14	23	15	16	17
4	4	4	4	4	4	4	4	4	4	4	10	4	4	4	4	4	4	4	4	4	6	4	24	24	22	14	23	15	16	17
4	4	4	4	4	4	4	4	4	4	4	11	4	4	4	4	4	4	4	4	4	6	4	24	24	22	14	23	15	16	17
4	4	4	4	4	4	4	4	4	4	4	4	4	4	4	4	4	4	4	4	4	6	4	24	24	22	14	23	15	16	17
4	4	4	4	4	4	4	4	4	4	4	4	4	4	4	4	4	4	4	4	4	6	4	24	24	22	14	23	15	16	17
24	24	24	24	24	24	24	24	24	24	24	24	24	24	24	24	24	24	24	24	24	6	24	24	24	22	14	23	15	16	17
24	24	24	24	24	24	24	24	24	24	24	24	24	24	24	24	24	24	24	24	24	6	24	24	24	22	14	23	15	16	17
14	14	14	14	14	14	14	14	14	14	14	14	14	14	14	14	14	14	14	14	14	6	14	14	14	14	14	23	15	16	17
4	4	4	4	4	4	4	4	28	28	28	28	28	28	28	28	28	28	28	28	28	28	4	4	4	4	4	23	15	16	17
4	4	4	4	4	4	4	4	27	4	4	4	4	4	4	4	4	4	4	4	4	4	4	4	4	4	4	23	15	16	17
4	4	4	4	4	4	4	4	5	4	4	4	4	4	4	4	4	4	4	4	4	4	4	4	4	4	4	23	15	16	17
26	26	26	26	26	26	26	26	26	26	26	26	26	26	26	26	26	26	26	26	26	26	26	26	26	26	4	23	15	16	17
13	13	13	13	13	13	13	13	13	13	13	13	13	13	13	13	13	13	13	13	13	13	13	13	13	13	13	13	13	13	17

Figure 12: THERMIX regions for the PBMR-200 in cards TX13

1219	1219	1219	1219	1219	1219	1219	1219	1219	1219	1219	1219	1219	1219	1219	1220	1220	1238	1264	1276	1276	1289	1289
1218	1218	1218	1218	1218	1218	1218	1218	1218	1218	1218	1218	1218	1218	1218	1220	1220	1239	1264	1276	1276	1289	1289
1217	1217	1217	1217	1217	1217	1217	1217	1217	1217	1217	1217	1217	1217	1217	1220	1220	1240	1264	1277	1277	1290	1290
1216	1216	1216	1216	1216	1216	1216	1216	1216	1216	1216	1216	1216	1216	1216	1220	1220	1241	1264	1277	1277	1290	1290
0	0	0	0	0	0	0	0	0	0	0	0	0	0	0	1221	1221	1242	1265	1278	1278	1291	1291
0	0	0	0	0	0	0	0	0	0	0	0	0	0	0	1221	1221	1243	1265	1278	1278	1291	1291
0	0	0	0	0	0	0	0	0	0	0	0	0	0	0	1222	1222	1244	1266	1279	1279	1292	1292
0	0	0	0	0	0	0	0	0	0	0	0	0	0	0	1222	1222	1245	1266	1279	1279	1292	1292
0	0	0	0	0	0	0	0	0	0	0	0	0	0	0	1223	1223	1246	1267	1280	1280	1293	1293
0	0	0	0	0	0	0	0	0	0	0	0	0	0	0	1223	1223	1247	1267	1280	1280	1293	1293
0	0	0	0	0	0	0	0	0	0	0	0	0	0	0	1224	1224	1248	1268	1281	1281	1294	1294
0	0	0	0	0	0	0	0	0	0	0	0	0	0	0	1224	1224	1249	1268	1281	1281	1294	1294
0	0	0	0	0	0	0	0	0	0	0	0	0	0	0	1225	1225	1250	1269	1282	1282	1295	1295
0	0	0	0	0	0	0	0	0	0	0	0	0	0	0	1225	1225	1251	1269	1282	1282	1295	1295
0	0	0	0	0	0	0	0	0	0	0	0	0	0	0	1226	1226	1252	1270	1283	1283	1296	1296
0	0	0	0	0	0	0	0	0	0	0	0	0	0	0	1226	1226	1253	1270	1283	1283	1296	1296
0	0	0	0	0	0	0	0	0	0	0	0	0	0	0	1227	1227	1254	1271	1284	1284	1297	1297
0	0	0	0	0	0	0	0	0	0	0	0	0	0	0	1227	1227	1255	1271	1284	1284	1297	1297
0	0	0	0	0	0	0	0	0	0	0	0	0	0	0	1228	1228	1256	1272	1285	1285	1298	1298
0	0	0	0	0	0	0	0	0	0	0	0	0	0	0	1228	1228	1257	1272	1285	1285	1298	1298
0	0	0	0	0	0	0	0	0	0	0	0	0	0	0	1229	1229	1258	1273	1286	1286	1299	1299
0	0	0	0	0	0	0	0	0	0	0	0	0	0	0	1229	1229	1259	1273	1286	1286	1299	1299
0	0	0	0	0	0	0	0	0	0	0	0	0	0	0	1230	1230	1260	1274	1287	1287	1300	1300
0	0	0	0	0	0	0	0	0	0	0	0	0	0	0	1230	1230	1261	1274	1287	1287	1300	1300
1232	1232	1232	1232	1232	1232	1232	1232	1232	1232	1233	1233	1234	1234	1234	1231	1231	1262	1275	1288	1288	1301	1301
1232	1232	1232	1232	1232	1232	1232	1232	1232	1232	1233	1233	1234	1234	1234	1231	1231	1263	1275	1288	1288	1301	1301
1235	1235	1235	1235	1235	1235	1235	1235	1235	1235	1235	1235	1235	1235	1235	1235	1235	1235	1237	1237	1237	1237	1237
1236	1236	1236	1236	1236	1236	1236	1236	1236	1236	1236	1236	1236	1236	1236	1236	1236	1236	1237	1237	1237	1237	1237

Figure 13: Final ID. Numbers of PBMR-200 VSOP-Batches

2.3.2.1 Neutron flux distribution

Printouts were requested for the thermal and fast neutron flux and the results are presented and analysed in Chapter 3.

2.3.2.2 Power density distribution

Printouts for the power density distribution were requested at 0 and at 200 bar partial steam vapour pressure for the PBMR-200. The results of the power density distribution are shown and analysed in Chapter 3.

3 VSOP 99/05 simulation results

This section presents the results for the start-up, burn-in and water ingress simulation done for the PBMR-400 and PBMR-200 reactor cores and comparison of the results.

3.1 Comparison of the PBMR-200 and PBMR-400 results

A general view of the effects of water ingress on the reactivity increase, the radial power profile and the thermal flux results, for both reactors being studied, will be discussed in this section.

3.1.1 Reactivity increase results

3.1.1.1 Reactivity increase results for the case of water ingress into the reflectors only

Figure 14 below compares k_{eff} as a function of partial steam vapour pressure during water ingress into only the reflectors for the PBMR-400 up to 400 bar and the PBMR-200 up to 300 bar.

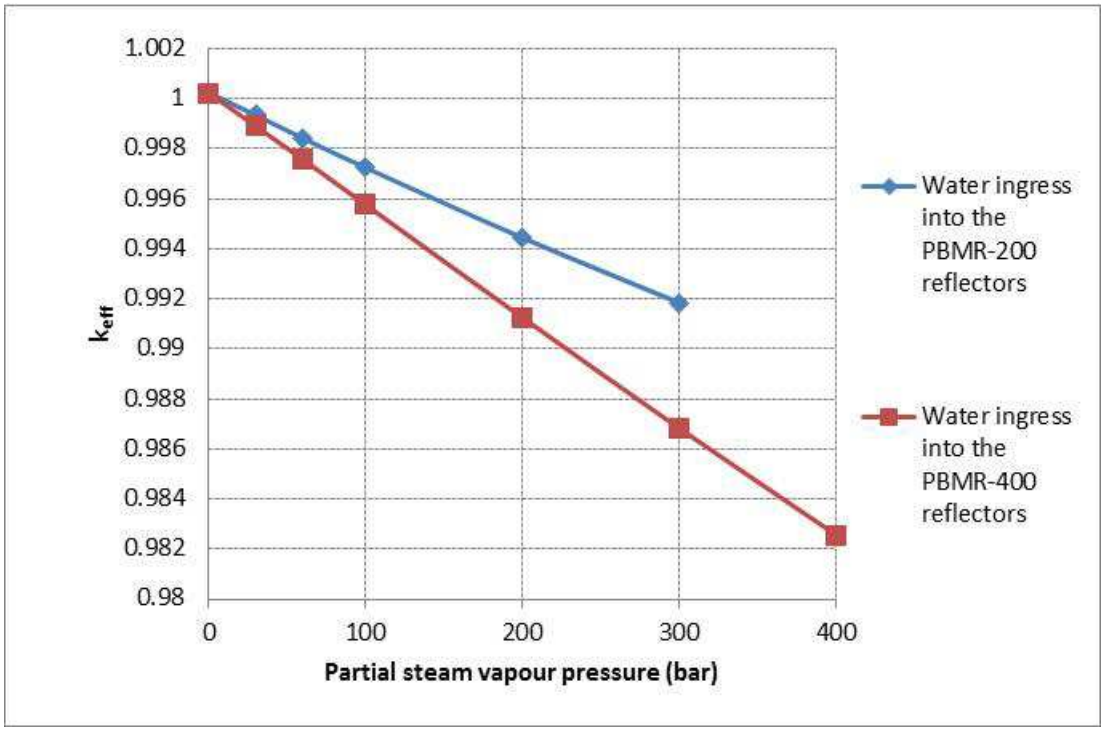

Figure 14: Comparison of the value of k_{eff} for the PBMR-200 and the PBMR-400, for the case of water ingress into the reflectors only

It can be observed from this figure that increasing water ingress into only the reflectors led to a substantial reduction in k_{eff}. This effect was about twice as large in the PBMR-400 as in the PBMR-200.

This negative reactivity effect of water ingress into the reflectors was probably caused by the fact that the neutrons in the reflectors were already strongly moderated before water ingress. Since, in the thermal region, σ_γ increases strongly with decreasing neutron energy, these well moderated neutrons in the reflectors will be captured much stronger by the ^1H, compared to the neutrons in the fuel core that are much less thermalised, due to the strong under-moderation in fuel. In the reflectors ingressing ^1H will also thermalise the already well thermalised neutron flux even more, which, by the same reasoning as above, can be expected to also increase the number of captures in the graphite.

The fact that k_{eff} decreased much more in the PBMR-400, for the same ingress of partial steam vapour pressure, can probably be explained by the much smaller distance of the average fuel sphere from the external reflector in the PBMR-400, compared to the PBMR-200: The fuel annulus in the PBMR-400 core is only 85 cm thick and thus all fuel spheres are situated between 0 cm and 85 cm from the inner boundary of the external reflector. However, in the PBMR-200 the radius of the fuel core is 150 cm and thus all fuel spheres are situated between 0 cm and 150 cm from the closest external reflector boundary. This much larger distance to the inner fuel spheres suggest that the influence of neutron captures in the external reflector will be much smaller in these inner fuel spheres in the PBMR-200. The fraction of the fuel core in which the thermal neutron flux, and thus the fission rate, will be suppressed due to the additional neutron captures induced by water ingress into the external reflector, will thus be significantly larger in the PBMR-400 than in the PBMR-200, which explains the larger reduction in k_{eff} in the PBMR-400.

3.1.1.2 Reactivity increase results for the case water ingress into the core only

Figure 15 compares k_{eff} as a function of partial steam vapour pressure during water ingress into the core only, for the PBMR-400 and the PBMR-200.

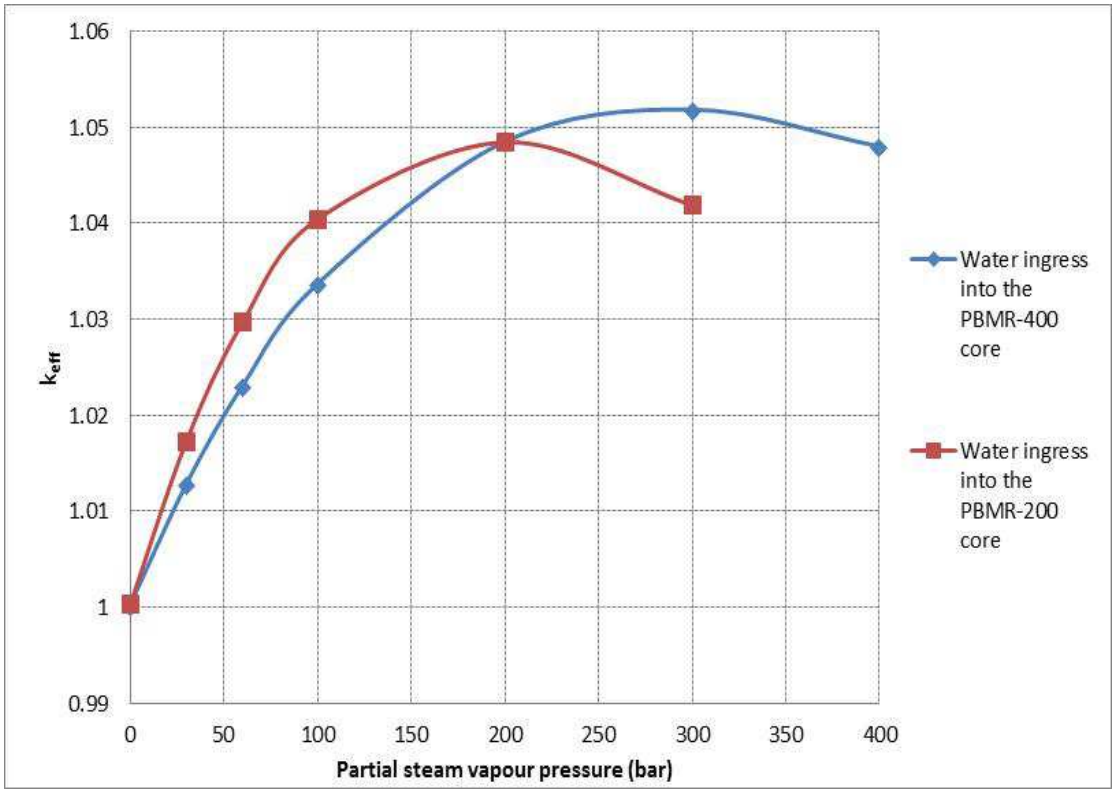

Figure 15: Comparison of the k_{eff} for the case of water ingress into the core only

It can be seen from the figure that the value of k_{eff} was initially significantly lower for the PBMR-400 than for the PBMR-200. However k_{eff} peaked at a lower partial steam vapour pressure for the PBMR-200 and thus the graphs cross over at about 200 bar. When water was added into the core, this probably led to faster neutron moderation in the fuel and thus a decrease in resonance capture by ^{238}U of neutrons in the process of slowing down. Therefore k_{eff} increased. The value of k_{eff} reached a maximum of 1.05184 in the PBMR-400, compared only 1.04843 in the PBMR-200 core after water ingress. This difference can probably be explained by the lower heavy metal (HM) loading of the fuel spheres for the PBMR-200: lower HM loading reduces the volume fraction of the coated fuel particles and thus increases the average distance between fuel kernels. Neutrons thus, on average, traverse longer path lengths of graphite between collisions with fuel kernels. The probability of getting moderated before being captured in the resonances of ^{238}U, i.e. the resonance escape probability, thus increases. Since less neutrons are now captured in the fuel, reducing these captures even further, by improving the moderation by means of water ingress, will thus cause a smaller increase in k_{eff}.

The peaking of the curves can probably be explained by a cross-over from under moderation to over moderation: Without water ingress into the fuel, the fuel is under

moderated in that the fuel free path lengths that the average neutron traverses through graphite between encounters with fuel kernels is too short to make the rate of moderation fast enough in order to reduce neutron capture in the epithermal resonances of ^{238}U to insignificant levels, i.e. the resonance escape probability will be significantly below 1.0 and thus k_{eff} will be significantly reduced because of these captures. As water ingress increases, the number density of ^{1}H between the fuel spheres, the moderation ratio will increase and thus the resonance escape probability will increase in the direction 1.0 and thus k_{eff} will increase. This explains the initial part of the curves where k_{eff} increases sharply with increasing partial water vapour pressure. However, at some point the moderation will become so effective that neutron capture in the resonances will fall to insignificant levels and thus the resonance escape probability will get very close to 1.0. From this point onwards increasing moderation will lead to only insignificant increases in k_{eff}, i.e. the curves will become flat. However, increasing water ingress beyond this point will lead to significant increases in the capture of thermalised neutrons in the ingressing ^{1}H, which will then start to reduce k_{eff}, i.e. the curve will have gone beyond its peak and will thus have crossed over from under to over moderation.

The fact that the curve for the PBMR-200 crosses over to over moderation before that of the PBMR-400 can probably be explained by the lower heavy metal loading in the PBMR-200. The PBMR-200 is thus initially less under moderated and will thus require less water ingress in order to cross over to over moderation.

3.1.1.3 Reactivity results for the case of water ingress into both the core and reflectors

The effect on the reactivity of simultaneous water ingress into both the core and reflectors is compared for the PBMR-400 and PBMR-200 in Figure 16 below. It can be observed that for the PBMR-200 k_{eff} initially climbs faster and has a higher peak of 1.044 compared to that of the PBMR-400 which has a peak of 1.041. The PBMR-200 reaches its peak at 200 bar and then drops to a k_{eff} value of 1.036 at 300 bar. For the PBMR-400, a maximum value of k_{eff} is reached only at about 300 bar and then drops to 1.034 at 400 bar.

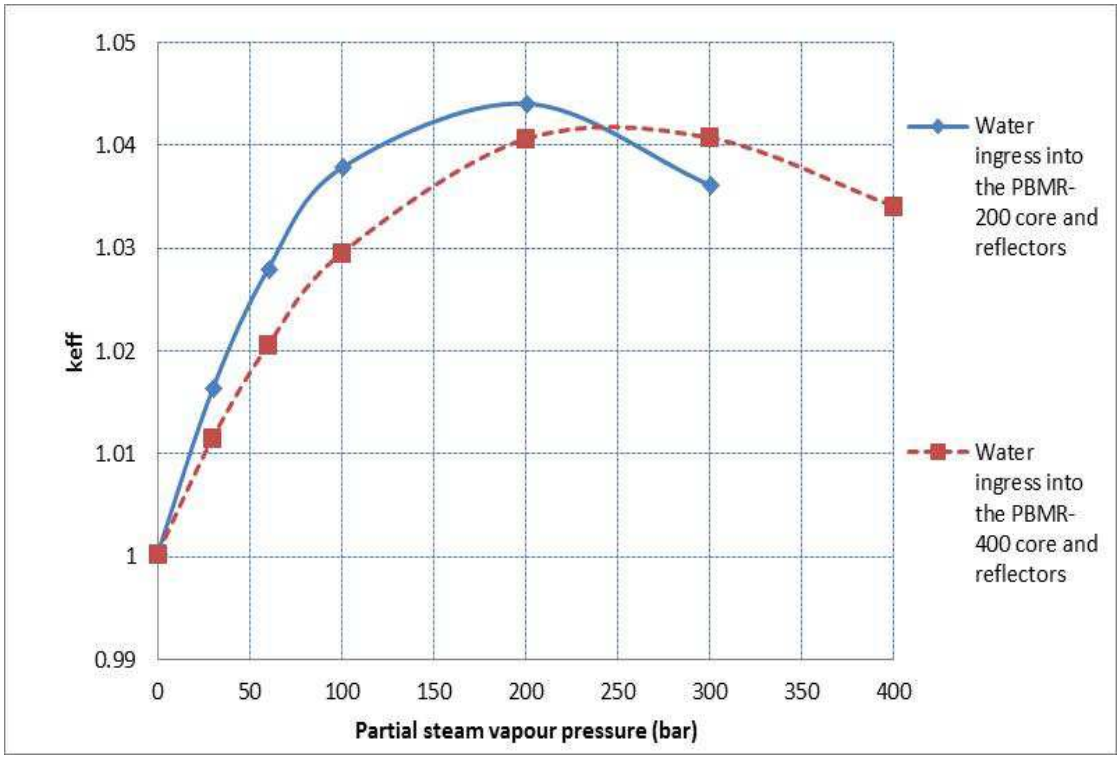

Figure 16: Comparison of reactivity increase for PBMR-200 and PBMR-400 for the case of water ingress into the core and reflectors

It is interesting to note that the PBMR-200 has now overtaken the PBMR-400 in that its peak k_{eff} is higher for water ingress into both the core and external reflector, while it was lower for ingress into only the core. This can be explained by the fact that the reduction in k_{eff} for water ingress into the external reflector only, was much higher for the PBMR-400. The nett effect of the opposing factors discussed above, i.e. improved moderation in the fuel versus increased neutron absorption in the graphite and ^{1}H in the reflectors, are assumed to be responsible for the reactivity increases in the two reactors as shown in Figure 16 above.

3.1.2 Neutron flux profiles

3.1.2.1 Thermal neutron flux profile distortions due to water ingress into the external reflectors only

Figure 17 below shows a comparison of the distorted radial thermal flux profiles for the PBMR-400 and PBMR-200 due to water ingress into the external reflector only, at 300 and 200 bar respectively, compared to the undistorted profiles before water ingress.

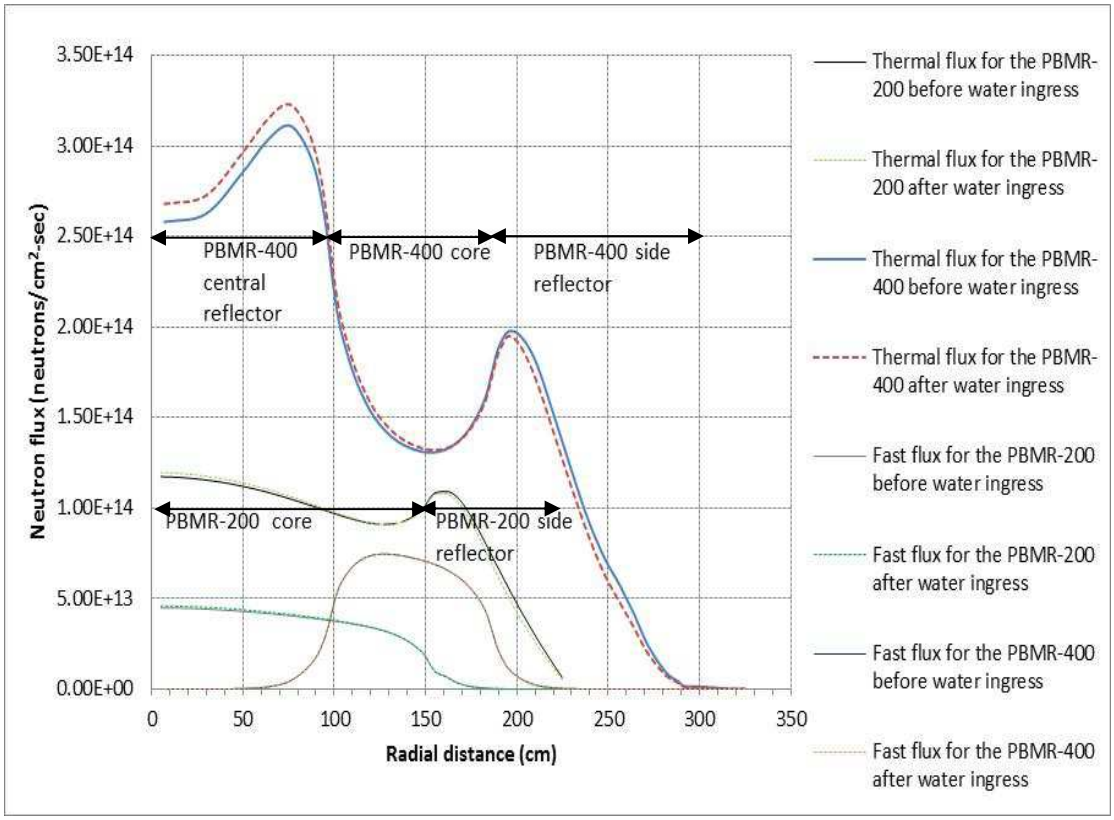

Figure 17: Distortion of the radial thermal flux profiles due to water ingress into the external reflector only at respectively 612 cm from the top of the core for the PBMR-400 and 374.40 cm from the top of the core for PBMR-200

It can be observed from Figure 17 that water ingress caused a relatively small decrease in the thermal flux in the external reflector and a substantial increase in the central reflector in the PBMR-400. The trend in the fuel core is similar, but almost too small to observe: close to the external reflector water ingress caused a slight decrease in thermal flux. This was probably due to reduced influx of thermal neutrons from the external reflector, due to the reduced flux there. This reduction in the flux in the fuel close to the external reflector then crossed over to a slight increase in the fuel close to the external reflector and to a more substantial increase in the internal reflector.

In the PBMR-200, the changes were even smaller, i.e. water ingress caused a slight decrease in the external reflector and the fuel close to it, which then crossed over to a slight increase in the middle of the fuel core.

It should be noted that these increases in thermal flux in the inner parts of the fuel cores do not represent actual reality, but is caused by the way VSOP approaches calculation of neutron flux in of sub- or super critical cores. In reality, inducing a

sustained sub-criticality of the reactor will always cause a continual reduction in neutron flux throughout the whole fuel core and thus in total power until the fission chain reaction is shut down. Similarly sustained super criticality will always cause an increase in flux and power. However, in its equilibrium mode, the power in VSOP is set to pre-determined fixed value which is artificially maintained despite deviations from criticality. This means that the flux is similarly maintained in an artificial manner. Therefore the reduction in thermal flux, and thus in power, in the external parts of the fuel core is by definition artificially countered by increasing this flux and power in the inner parts of the fuel core, in order to maintain the total power at the fixed value. This increase in the fission rate in the inner part of the fuel core then produces more fast neutrons which then leak into the internal reflector where they are moderated, thus causing the observed increased thermal flux in the central reflector of the PBMR-400.

The fact that the increase in thermal flux in the internal reflector is larger than the decrease in thermal flux in the external reflector, is counter intuitive and can possibly be explained as follows: in the external reflector the water ingress causes the opposing effects of faster moderation of fast and epithermal neutrons, which will tend to increase the thermal flux, and increased capture of these thermal neutrons, both by the ^{1}H and graphite, which will tend to reduce the thermal flux. To the extent that these opposing effects cancel each other out, the change in thermal flux will then be very small. However, as far as fast neutrons are concerned, the only major force at work will be faster moderation by the ^{1}H.

It should, however, be noted that the changes VSOP makes to the neutron flux in order to artificially maintain the total reactor power at the preset value, do not all have to take place in the radial profile, but can happen in any region of the core. That this is the case is demonstrated by the distortions in the axial power profiles at 5 cm into the radial distance of the core in Figure 18 and Figure 19 below for water ingress into the external reflector only.

Figure 18 may also explain why the observed distortions in the radial thermal flux profiles for the PBMR-200 in Figure 17 were so small: one would expect the increased thermal neutron capture due to water ingress into the external reflector to reduce the thermal flux in the fuel too. However, at the axial position of 374.40 cm and 328.40 cm, respectively from the top of the core of the radial profiles, Figure 18 shows an increase in the axial thermal neutron flux profile. If the radial profiles were thus taken near the top or bottom of the core, where Figure 18 shows a reduction in the thermal flux, the expected large reductions in the radial thermal flux profiles

would probably have been observed. This shows that the influence of water ingress is determined by the balance of a number of complex and opposing and forces, so that their combined effect cannot be explain in a simplistic manner.

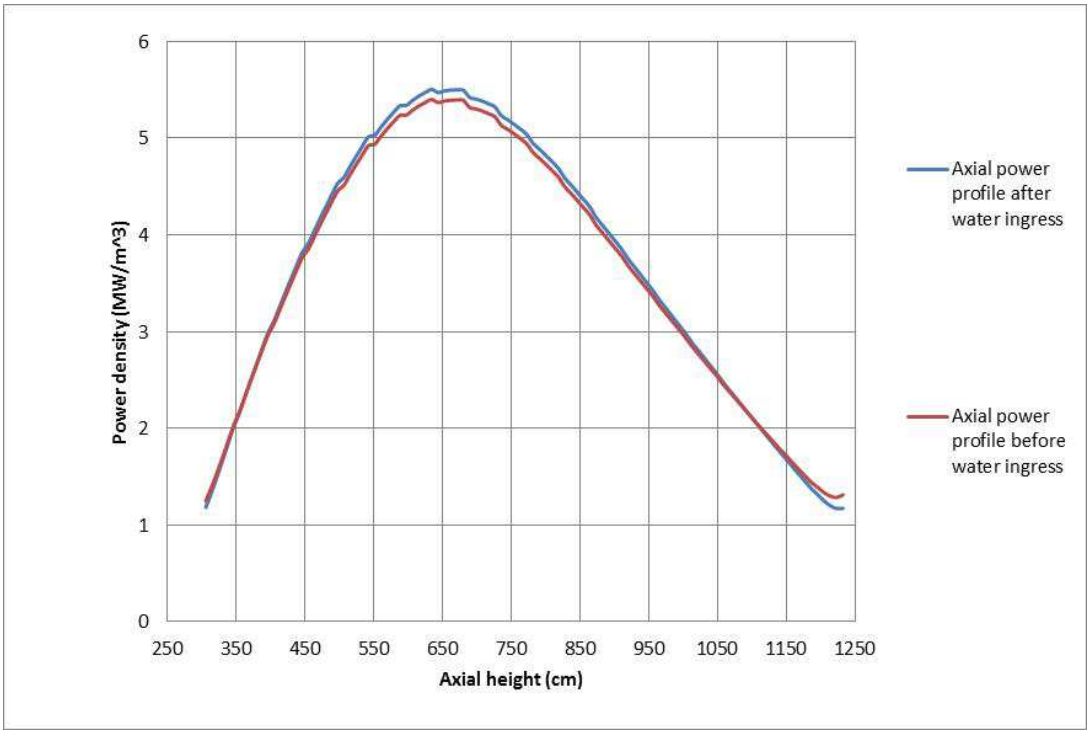

Figure 18: Axial power distortion due to water ingress into the PBMR-200 external reflectors only

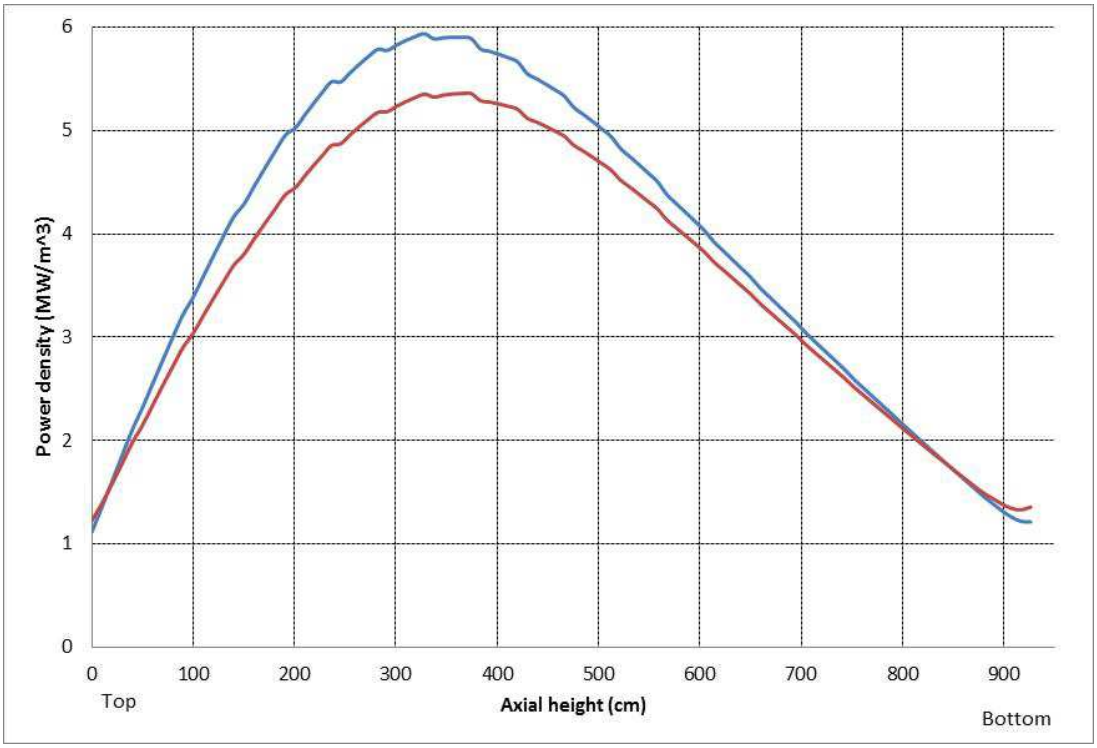

Figure 19: Axial power distortion due to water ingress into the PBMR-200 core only

3.1.2.2 Thermal neutron flux profile distortions due to water ingress into the core only

Figure 20 below shows the effect of water ingress into the core only on the thermal neutron flux. The fluxes for the PBMR-400 shown were taken at 300 bar and 612 cm from the top of the core. For the PBMR-200, the thermal fluxes were taken at 374.40 cm from the top of the core at 200 bar partial steam vapour pressure.

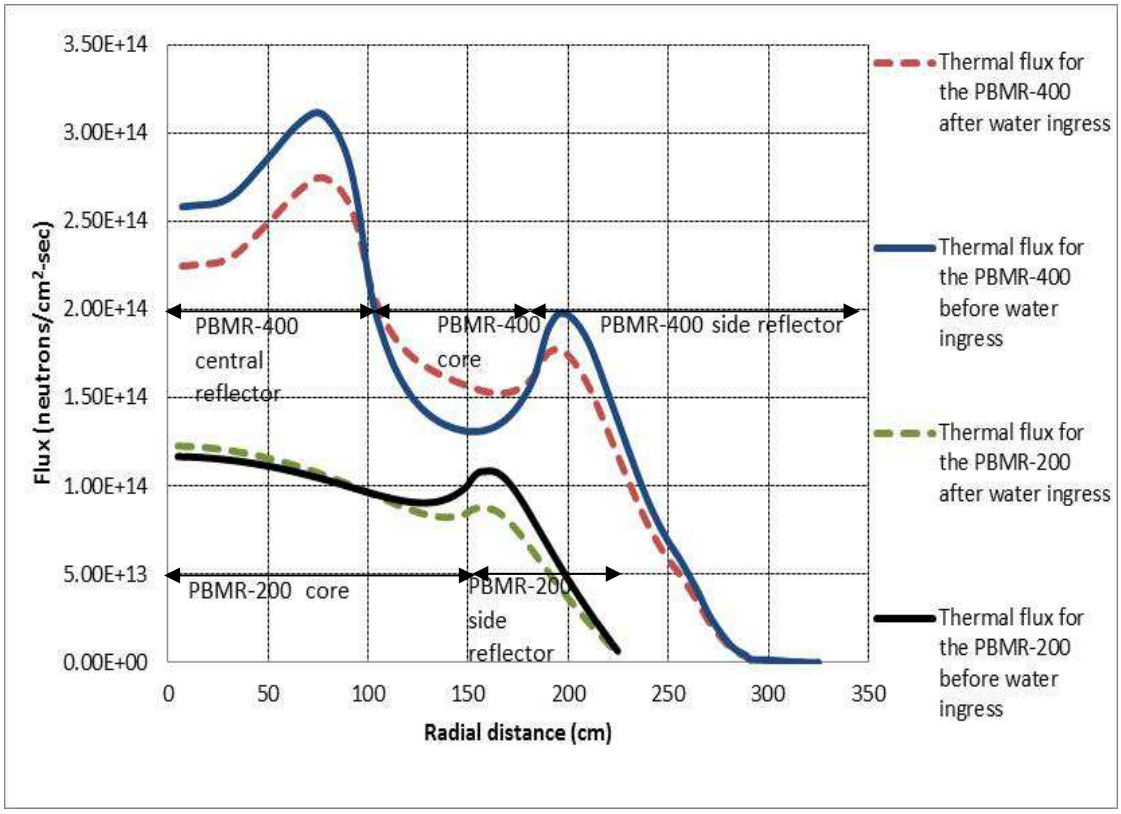

Figure 20: Radial profiles for the thermal flux distribution for the case water ingress into the core only

It can be observed that the water ingress substantially increased the thermal neutron flux in the centre of the PBMR-400 fuel core, but then it gradually crossed over to a slight reduction in the parts of the core close to both the internal and external reflectors and then to a substantial reduction in these reflectors. In the PBMR-200, the flux is observed to increase at the centre of the fuel core after water ingress and decrease towards and in the external reflector.

Once again it should be noted that the induced super-criticality would in reality lead to flux increases throughout the core, but that VSOP's renormalisation of the power leads to flux reductions away from the central parts of the fuel core. The cross-over from an increased flux in the central parts of the fuel core to a decrease near and

inside the reflectors can probably be explained by reduced leakage of fast and epithermal into the reflectors: faster moderation of fast and epithermal neutrons in the fuel core, due to water ingress there, will by definition reduce the number of fast and epithermal neutrons that remain in the core and is thus available to leak into the reflectors. This reduced influx of fast and epithermal neutrons into the reflectors will then reduce the number of neutrons available for thermalisation in the reflectors and thus the thermal flux there.

3.1.2.3 Thermal neutron flux profile distortions due to water ingress into both the core and external reflectors

Figure 21 below compares the water ingress effect into both the core and reflectors for the PBMR-400 and the PBMR-200. The fluxes for the PBMR-400 shown were taken at 300 bar and 612 cm from the top of the core. For the PBMR-200, the thermal fluxes were taken at 374.40 cm from the top of the core at 200 bar partial steam vapour pressure.

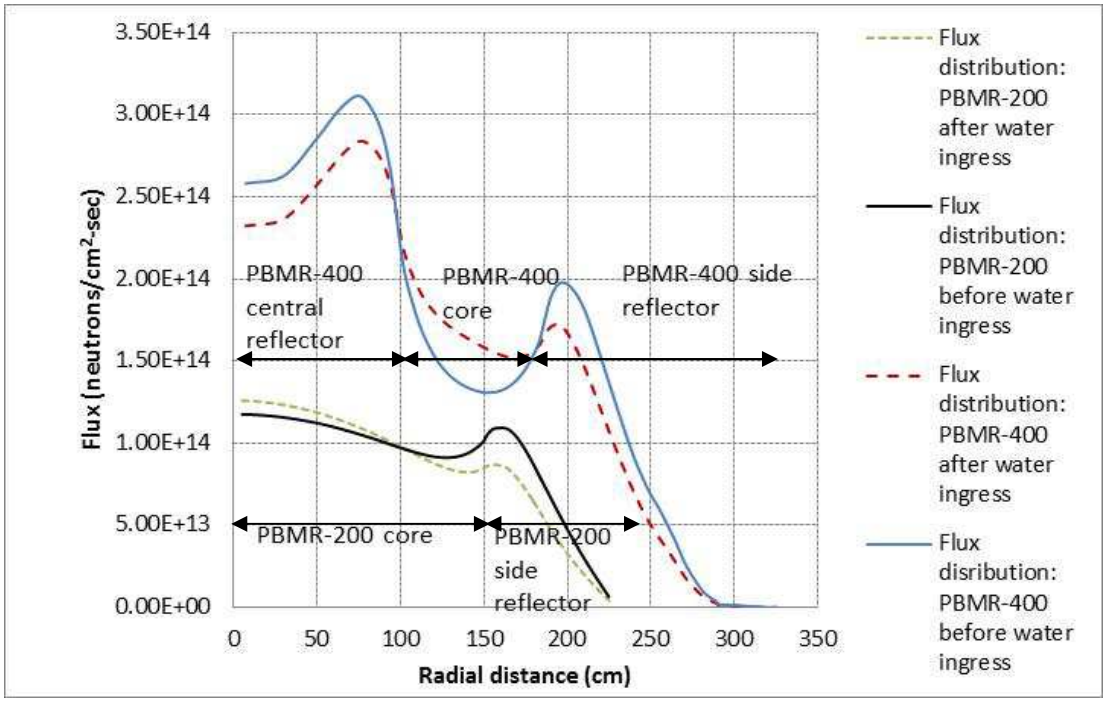

Figure 21: Comparison of the effect of water ingress into both the core and reflectors on thermal flux profiles

It can be seen that for both reactors when both ingresses are combined, this causes a substantial increase in the thermal flux in the inner regions of the fuel core, which then cross over to substantial reductions in the reflectors and lesser reductions in the fuel directly adjacent to it.

The distortion of the flux profiles due to water ingress into both the core and reflector is similar to that of water ingress into only the core as discussed above in section 3.1.2.3.

3.1.3 Power density distribution

In this section the radial power density distributions for the cases of water ingress into the reflector only, the core only and water ingress into both the core and reflectors for the PBMR-400 and PBMR-200 will be compared.

3.1.3.1 Power density distribution results for the case of water ingress into the reflectors only

Figure 22 below shows a comparison of the radial power profile for the PBMR-400 and the PBMR-200 due to water ingress into the reflectors only.

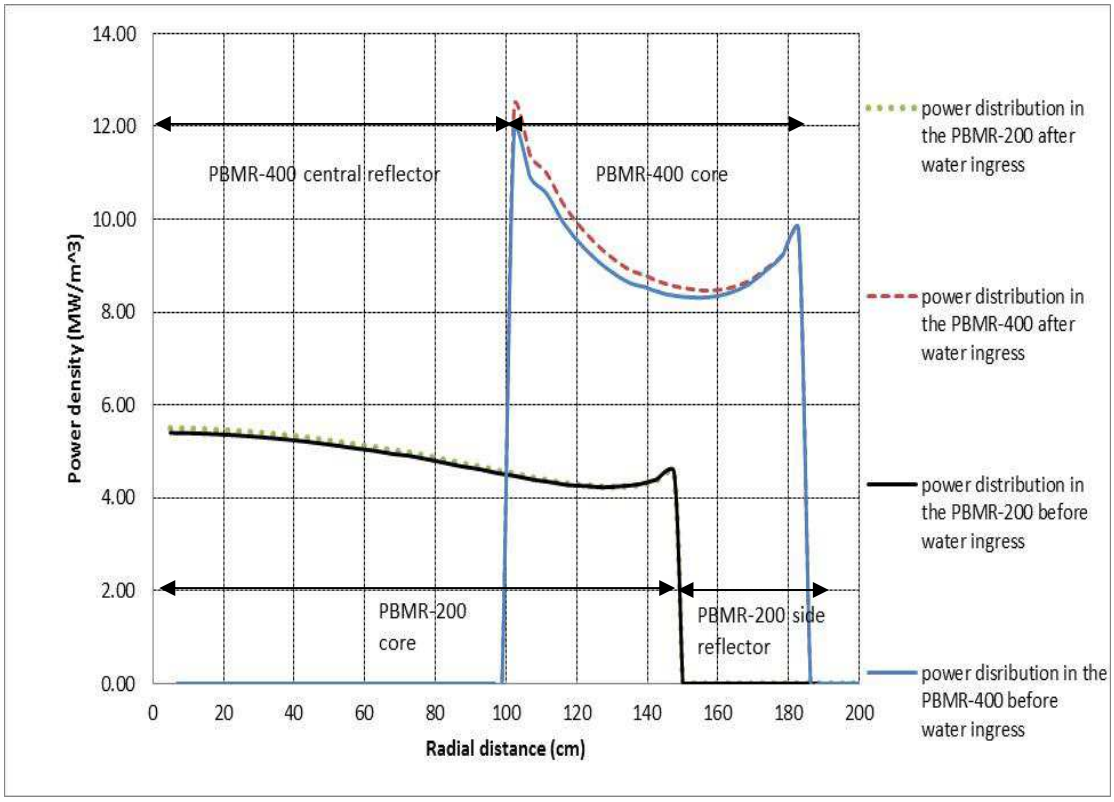

Figure 22: Comparison of the effect of water ingress into only the external reflector on the radial power distribution

From this figure it can be seen that water ingress into the external reflector of the PBMR-400 produced only a tiny reduction in power in the fuel close to the external reflector and a slightly larger increase closer to the internal reflector and produced a similar, but even smaller, effect for the PBMR-200. Once again it should be noted

that this effect is not totally real but is partly produced by the artificial fixing of the total power in VSOP's equilibrium mode.

3.1.3.2 Power density distribution results for the case of water ingress into the core only

Figure 23 below, shows the distortion of the radial power profiles as a result of water ingress into only the fuel core.

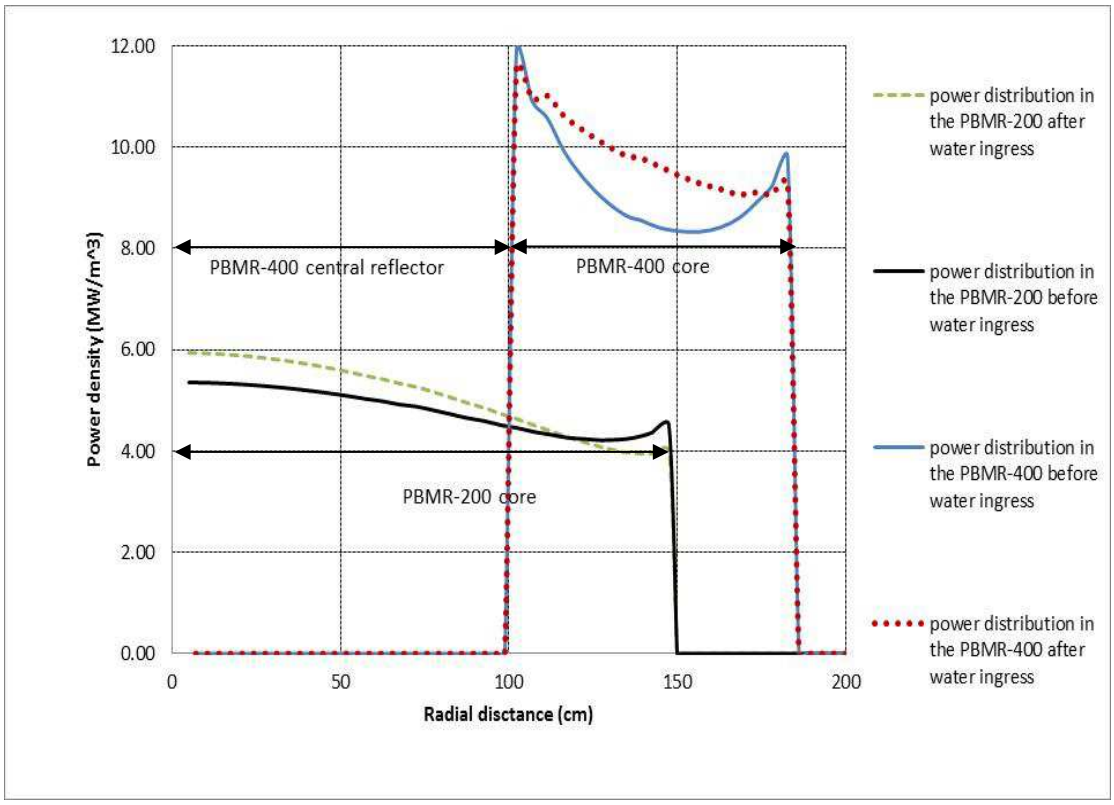

Figure 23: Comparison of the effect of water ingress into the core on the radial power distribution

The power density was seen to exhibit similar behaviour to that shown by the thermal neutron flux in the core. The power density increased in both cores after water ingress and crossed over to a slight reduction in PBMR-400 towards the side reflector.

3.1.3.3 Power density distribution results for the case of water ingress into the core and reflectors

Figure 24 below shows a comparison of radial power profiles for the PBMR-400 and the PBMR-200 due to water ingress into both the core and reflectors.

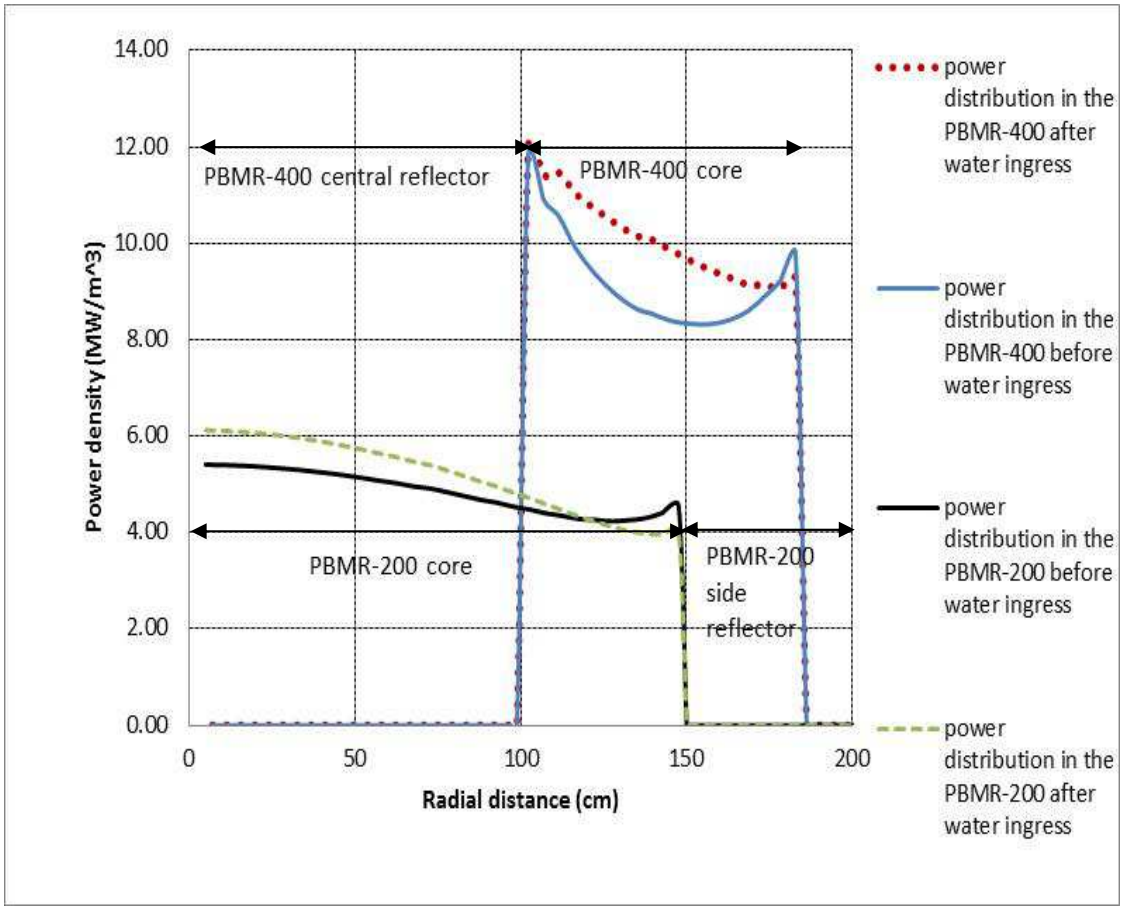

Figure 24: Comparison of the effect of water ingress into the core and reflectors on the radial power distribution

3.2 Detailed analysis of mechanisms driving reactivity changes due to water ingress

Reactivity increase results for water ingress into the external reflector only, the core only and both the core and the reflector for the PBMR-400 are shown in Table 6 below.

Table 6: k_{eff} results after water ingress in the PBMR-400

Partial Steam vapour pressure (bar)	Core only Δk_{eff} %	Reflectors only Δk_{eff} %	Core and Reflectors Δk_{eff} %
30	1.258710	-0.132969	1.129740
60	2.283475	-0.265939	2.029533
100	3.344231	-0.446897	2.927327
200	4.825890	-0.897794	4.038071
300	5.159813	-1.340692	4.051068
400	4.775902	-1.766594	3.385221

It can be observed from this table that when water ingress was simulated in the core only, the reactivity increased up to a maximum of 5.15% at 300 bar and then decreased to 4.77% at 400 bar. Water ingress into the reflectors caused a decrease in the value of Δk_{eff}% up to -1.77% when 400 bar of steam was added.

Reactivity increase results for water ingress into the reflector only, the core only and both the core and the reflector for the PBMR-200 are shown in Table 7 below.

Table 7: k_{eff} results after water ingress in the PBMR-200

Partial steam vapour pressure (bar)	Core Δk_{eff} %	Reflectors Δk_{eff} %	Core and reflectors Δk_{eff} %
30	1.700592	-0.089978	1.604615
60	2.939295	-0.181956	2.768336
100	4.015036	-0.299928	3.755099
200	4.817844	-0.579861	4.381948
300	4.161001	-0.839798	3.591138

It can be observed from this table that when water ingress was simulated in the core only, the reactivity increased up to a maximum of 4.81% at 200 bar and then decreased to 4.16% at 300 bar. Water ingress into the reflectors caused a decrease in the value of $\Delta k_{eff}\%$ up to -0.84% when 300 bar of steam was added.

The mechanisms that drive these changes in reactivity will be studied in order to obtain a thorough understanding of the process, which may lead to design changes that can mitigate these changes. The individual components that contribute to the following parameters, which contribute to the value of k_{eff}, will be studied:

1. Fuel utilisation, i.e. % neutrons absorbed in fissile fuels.
2. Core neutrons absorbed in non-fissile nuclides.
3. Leakage from the core (these end up leaking out of the pressure vessel or captured in the reflectors, pressure vessel, control rods etc).
4. The number of fission source neutrons emitted per neutron absorbed in the fissile fuel (η).

3.2.1 Neutron production by fissile isotopes

Figure 25 below compares neutron production by fissile isotopes for the PBMR-400 and the PBMR-200 as a function of partial steam vapour pressure during water ingress into the external reflector only. The plots were done only for selected fissile isotopes that showed significant percentage values i.e. ^{235}U, ^{239}Pu- and ^{241}Pu.

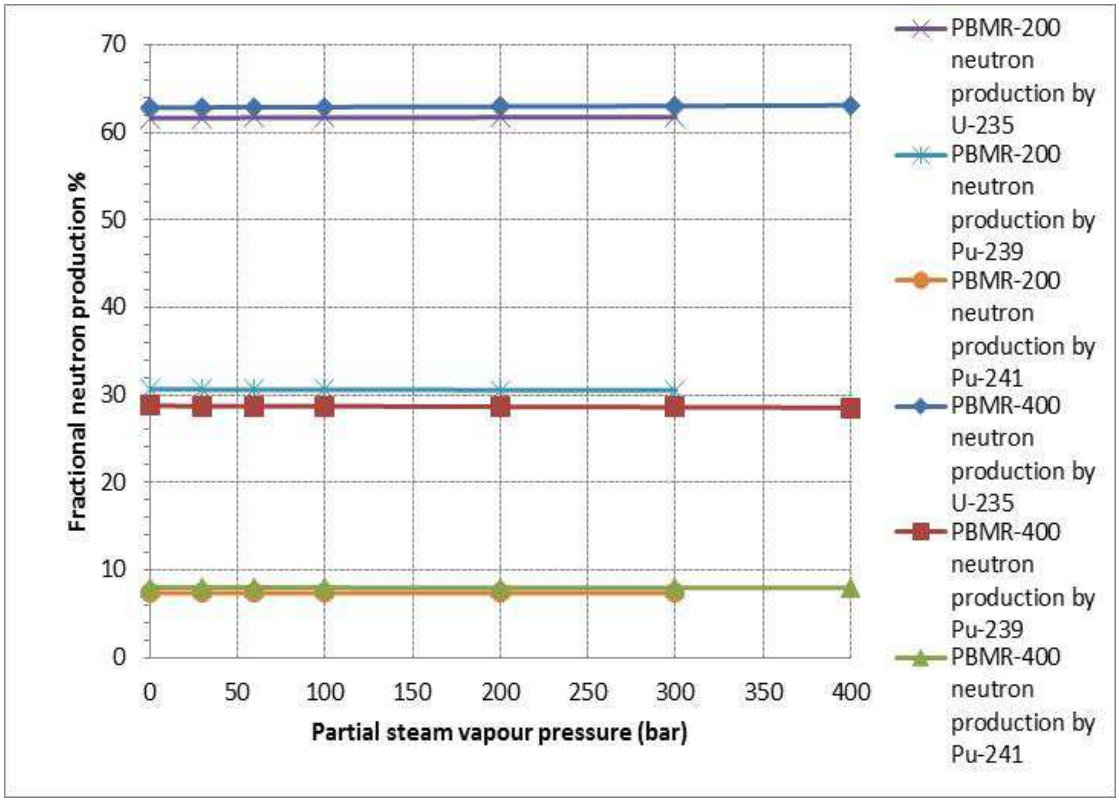

Figure 25: Neutron production by fissile isotopes after water ingress into the reflectors only

It can be seen from this figure that there was only small changes in the fractional production percentages when water was added into the reflectors for both the PBMR-400 and PBMR-200.

Figure 26 below shows the distortion of the neutron production by fissile isotopes for the PBMR-400 and the PBMR-200 as a function of partial steam vapour pressure during water ingress into the core only.

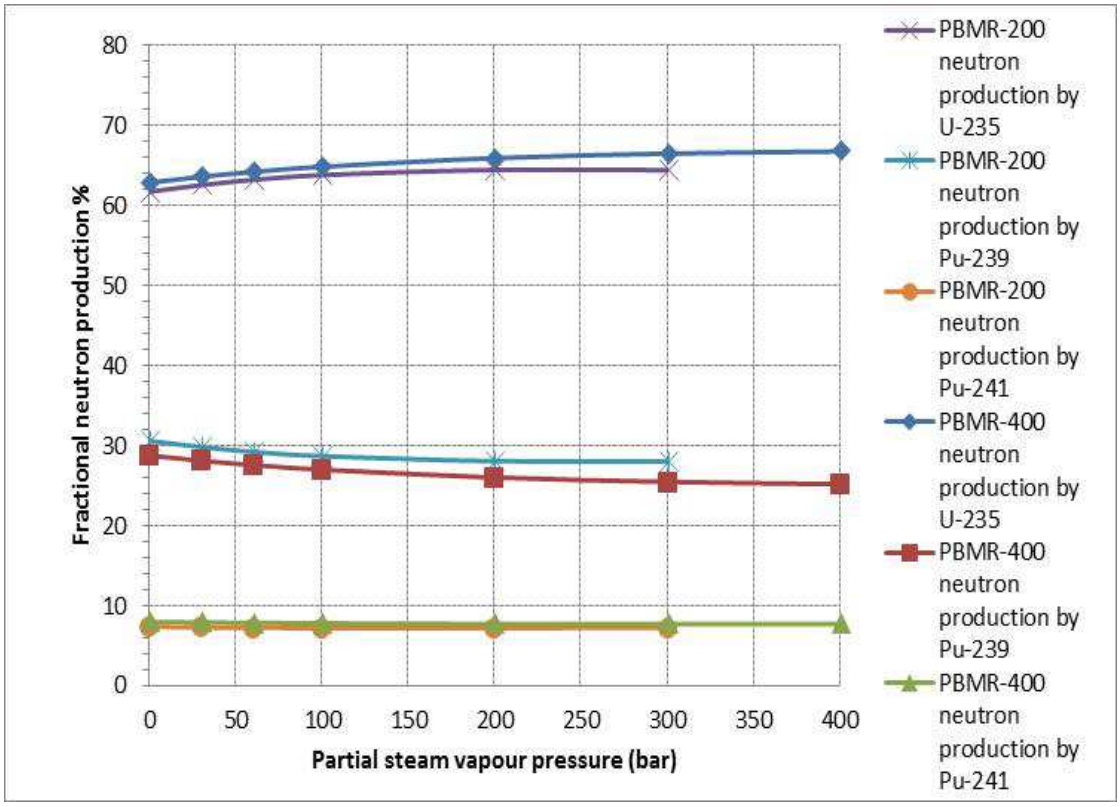

Figure 26: Neutron production by fissile isotopes after water ingress into the core only

From this figure, it can be seen that water ingress into the core led to a substantial increase in the fractional neutrons produced by ^{235}U. For the PBMR-200 ^{235}U neutron production increased by 2.7% while the PBMR-400 increased by 3.89%. The ^{239}Pu neutron production decreased substantially for both the PBMR-400 and PBMR-200 cores by 3.57% and 2.56% respectively.

It is not immediately clear what drove this swing from neutron production due to fissioning of ^{239}Pu to that of ^{235}U. One possibility is the influence of the thermal fission resonance of ^{239}Pu at 0.3 eV, as was discussed by Serfontein (2011: Figure 25). Since this resonance lies well above the peak of the Maxwellian energy spectrum of the thermalised neutron flux at normal operating temperatures, very few thermalised neutrons will produce fission in this resonance. However, neutrons that are already in the thermal energy window, but that are still in the process of being slowed down to thermal energies, may well produce fissions in this resonance. Therefore faster moderation, due to water ingress into the fuel core, may cause more neutrons to escape this fission resonance by being thermalised before being able to produce fission in this resonance. Such a mechanism will thus reduce fissions in this ^{239}Pu fission resonance and will correspondingly increase fissions at well thermalised, i.e. lower, energies in all the fissile fuels. However, since the number density of ^{235}U is much larger than that of ^{239}Pu, such a shift to lower energies may favour fission in

^{235}U. However, this unexpected result will be referred to the list of suggested future studies, rather than to analyse it further here.

Figure 27 below shows the distortion of the neutron production by fissile isotopes for the PBMR-400 and the PBMR-200 as a function of partial steam vapour pressure during water ingress into both the core and external reflector.

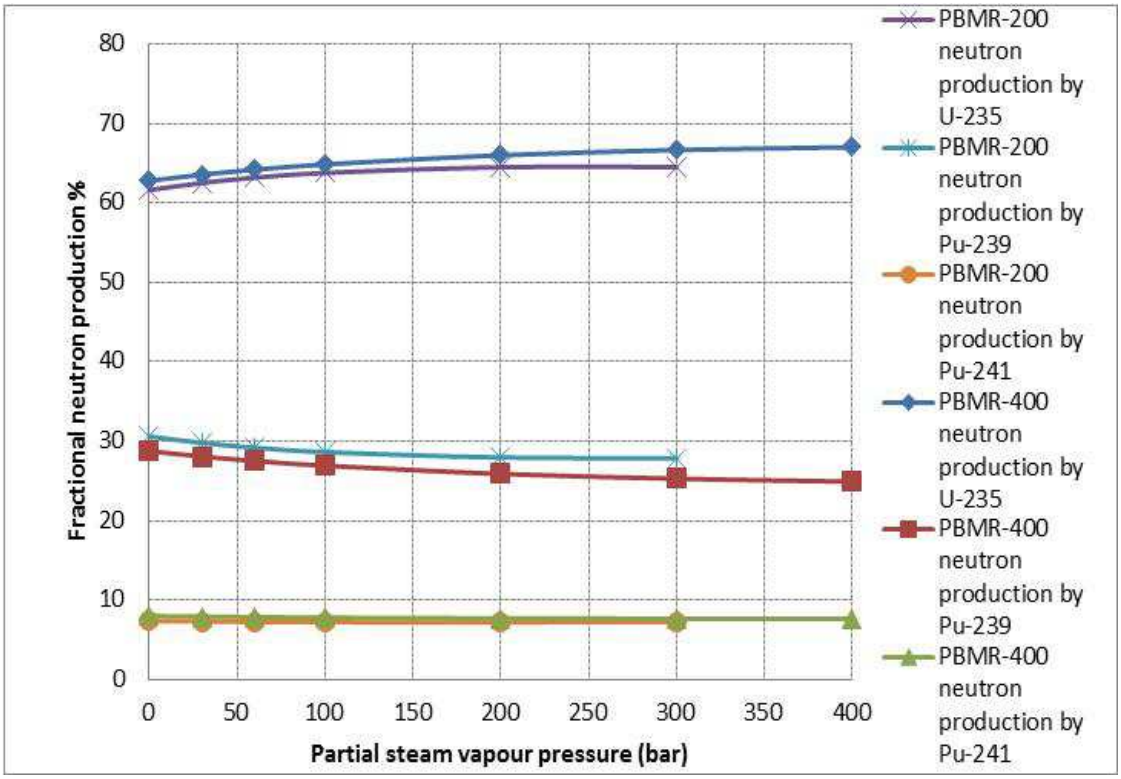

Figure 27: Neutron production by fissile isotopes after water ingress into the core and reflector

Similar to the above case of water ingress into the core only, the PBMR-400 ^{235}U is higher than the PBMR-200 case (4.22% vs only 2.89% for the PBMR-200). For ^{239}Pu fractional neutron production, the PBMR-400 value decreased by 3.83% while for the PBMR-200 it was 2.72%.

3.2.2 Neutron losses in heavy metals and fission products

This section will investigate the influence of water ingress on neutron losses in heavy metals, fission products and leakage out of the fuel core, which obviously all directly affect k_{eff}. This will be done for the case of water ingress into the fuel core only, into the external reflector only and into both the core and reflector, for both reactors.

Figure 28 below shows neutron losses in fissile isotopes, capture by fertile isotopes, losses in fission products and losses due to leakage for the PBMR-400, as a function of partial steam vapour pressure after water ingress into the reflectors only.

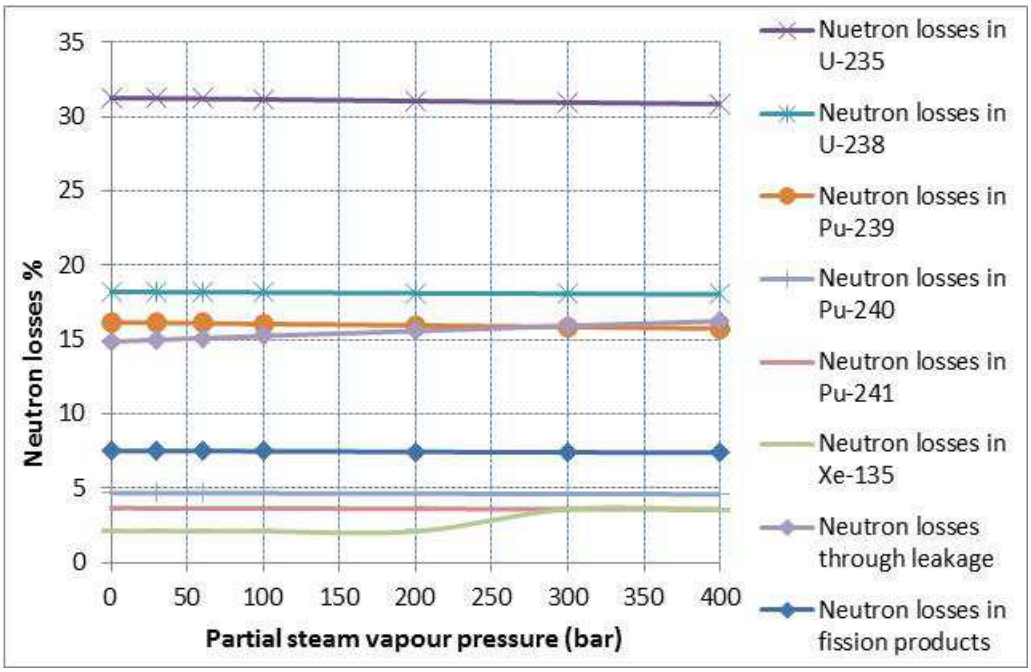

Figure 28: Neutron losses in the PBMR-400 after water ingress into the reflectors only

From Figure 28 above, it can be observed that in the case of water ingress into the reflector only, there was very little change in most of the neutron loss parameters. However, core leakage increased by 1.37%. This was to be expected since, as has been explained above, water ingress will increase neutron capture in both the ingressing ^{1}H and in the graphite in the external reflector: VSOP will allocate both these losses to the core leakage parameter. Neutron losses through capture in ^{135}Xe also increased by 1.46%. Both these factors will decrease k_{eff}. While the magnitude of these changes may seem small, it should be remembered that, a change in 1% in k_{eff} is viewed as very significant and that therefore these changes are also very significant.

Figure 29 below shows neutron losses in fissile isotopes, capture by fertile isotopes, captures in fission products and losses due to leakage for the PBMR-200, as a function of partial steam vapour pressure after water ingress into the reflector only.

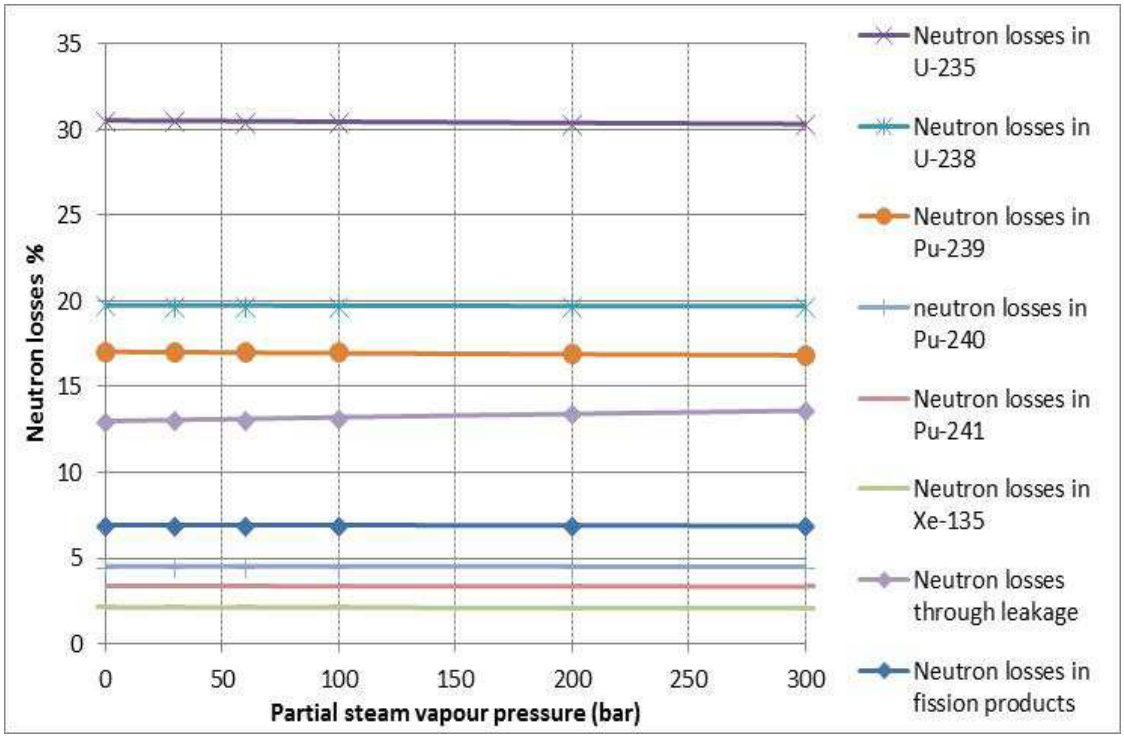

Figure 29: Neutron losses in the PBMR-200 after water ingress into the reflectors only

Most of the parameters for neutron loss showed no significant change except for core leakage which was seen to increase by 0.61%. The changes were thus less pronounced than for the PBMR-400. This corresponds to the reduction in k_{eff} that also was about 50% smaller for the PBMR-200 than for the PBMR-400.

Figure 30 below shows neutron losses in fissile isotopes, capture by fertile isotopes, capture in fission products and losses due to leakage for the PBMR-400, as a function of partial steam vapour pressure due to water ingress into the core only.

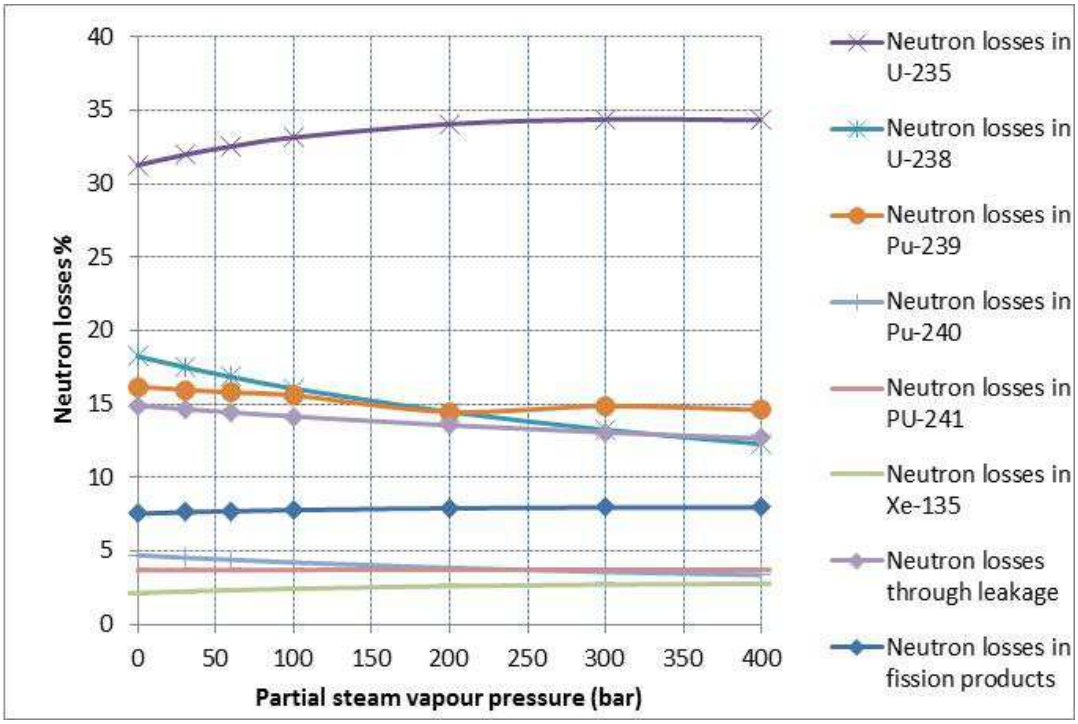

Figure 30: Neutron losses in the PBMR-400 after water ingress into the core only

From this figure, it can be observed that neutron loss, mainly by capture in the epithermal resonances, in ^{238}U decreased by 5.97% thereby substantially increasing the resonance escape probability and thus increasing the number of neutrons available for fission and thus substantially increasing the number of thermalised neutrons available to produce fission in the fissile nuclides. As this change predicted, the neutron loss by absorption in ^{235}U increased by 3.06% which means more fission reactions. This was partially countered by a smaller reduction in the neutron losses in ^{239}Pu, which suggests slightly less fissions. The core leakage also decreased by 2.23%, which means a substantial increase in the number of neutrons remaining in the core and which thus remains available for producing more fissions. To this should be added a small decrease in the losses in the fertile ^{240}Pu, of which most would be captures. All these factors would add to a combined strong increase in k_{eff}.

These positive factors were only countered by small increases in neutron losses in fission products and in ^{135}Xe. The combination of all these factors would thus suggest a large increase in k_{eff}, as was actually shown in Figure 15 and Figure 16 above.

Figure 31 below shows the distortion of the neutron losses PBMR-200 as a function of partial steam vapour pressure during water ingress into the core only.

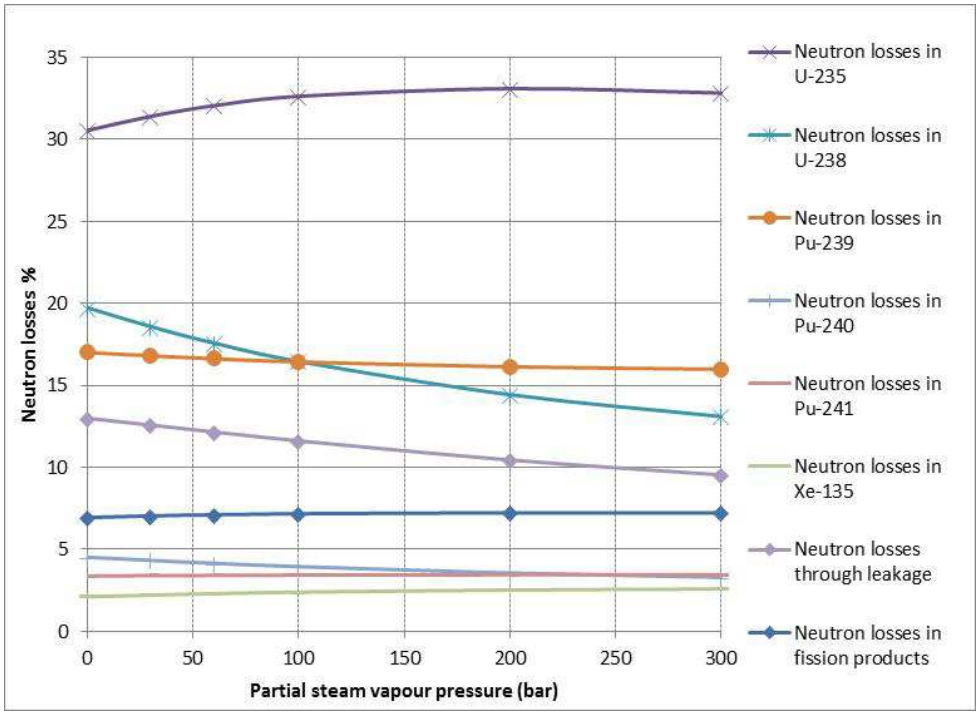

Figure 31: Neutron losses in the PBMR-200 after water ingress into the core only

From this figure, it can be observed that the neutron loss by absorption in ^{235}U increased by 2.28% which is about 1% less than that of the PBMR-400. The neutron loss by absorption in ^{238}U decreased by 6.64% thereby increasing the number of neutrons available for fission. The core leakage decreased by 3.46%. The tendencies are thus similar to that observed in the PBMR-400, but less pronounced, which corresponds to the smaller increase in k_{eff} which was shown above.

Figure 32 below shows the distortion of the neutron losses in the PBMR-400 as a function of partial steam vapour pressure during water ingress into both the core and external reflector.

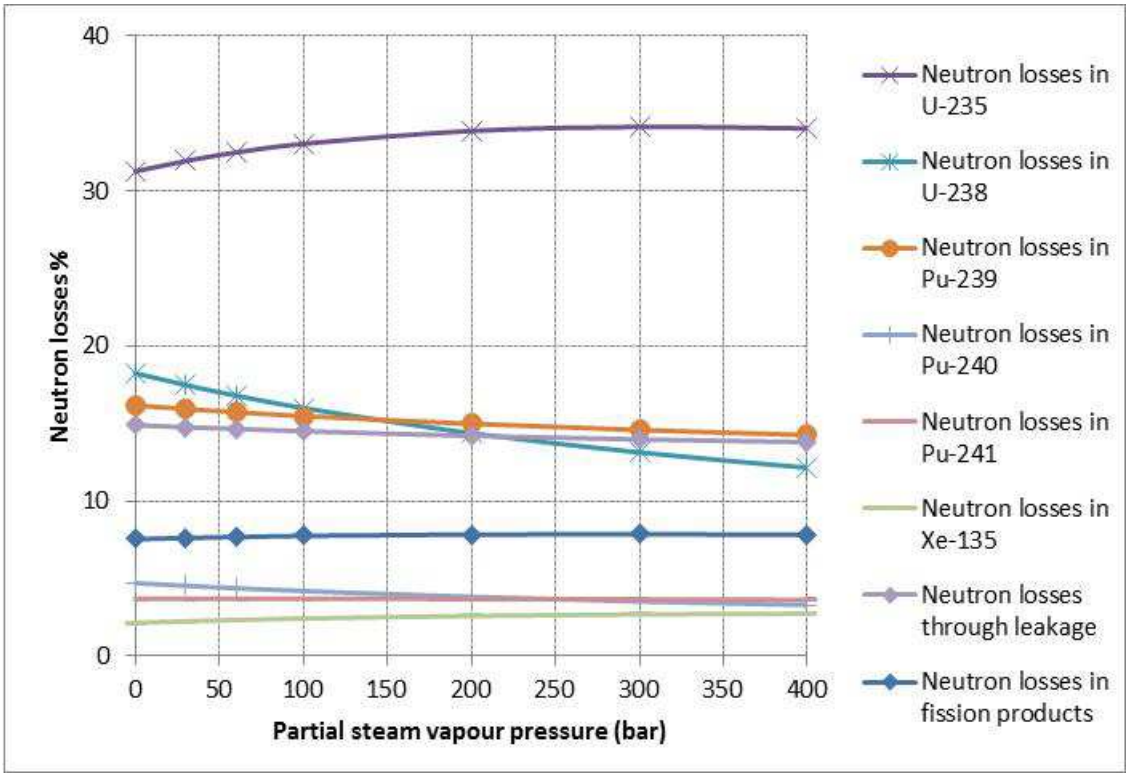

Figure 32: Neutron losses in the PBMR-400 after water ingress into the core and reflectors

From this figure, it can be observed that neutron loss by radiative capture in ^{238}U decreased by 6.1%. This neutron loss led to a substantial increase in the resonance escape probability and thus increasing the number of neutrons available for fission and thus substantially increasing the number of thermalised neutrons available to produce fission in the fissile nuclides. The result of the increase in fission neutrons is seen in the neutron loss by absorption in ^{235}U increased by 2.8%. The core leakage only decreased by 1.09%, which means a large number of neutrons remained in the core for producing more fissions. These factors would add to a combined strong increase in k_{eff}.

Figure 33 below shows the distortion of the neutron losses in the PBMR-200 as a function of partial steam vapour pressure during water ingress into both the core and reflector.

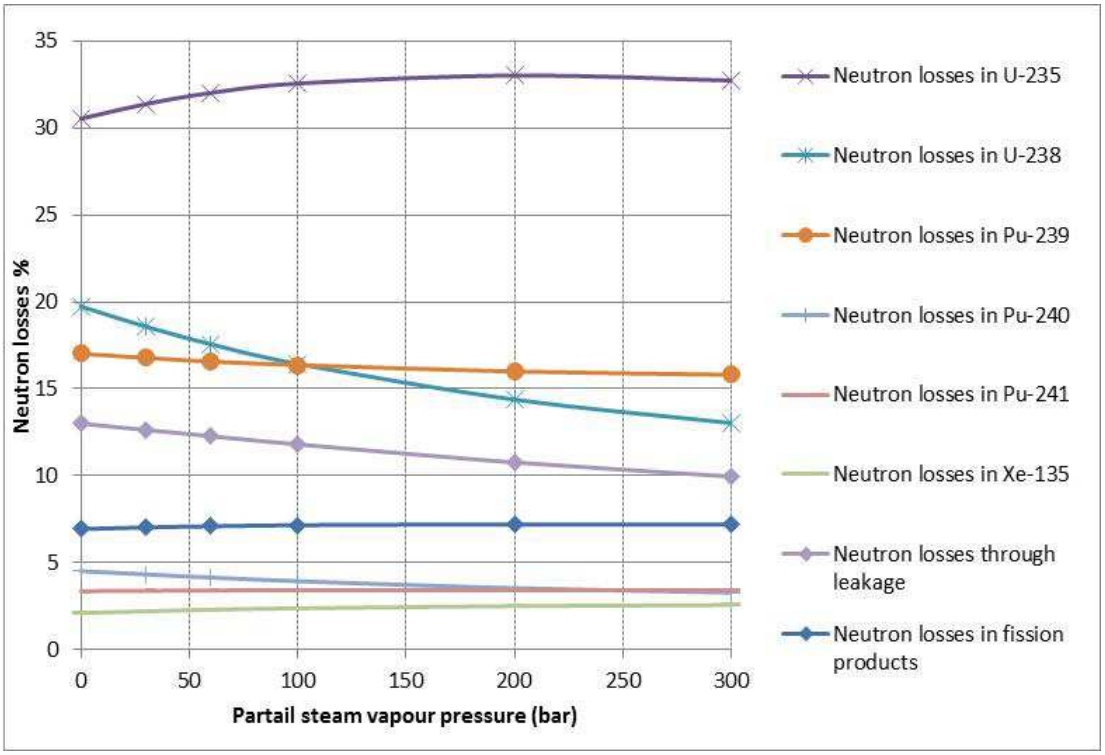

Figure 33: Neutron losses in the PBMR-200 after water ingress into the core and reflectors

From this figure, it can be observed that the neutron loss by absorption in ^{235}U increased by 2.2%. The neutron loss by absorption in ^{238}U decreased by 6.71% thereby increasing the number of neutrons available for fission. The core leakage decreased by 3.04% which decreased 2.5% more than that of the PBMR-400 hence the smaller increase in PBMR-200 k_{eff}.

3.2.3 Fission source neutrons emitted per neutron absorbed

Figure 34 below compares distortion of the fission source neutrons emitted per neutron absorbed in fissile nuclides (η) for the PBMR-400 and the PBMR-200, as a function of partial steam vapour pressure, for different ingress scenarios, i.e. into the external reflector only, fuel core only and into both .

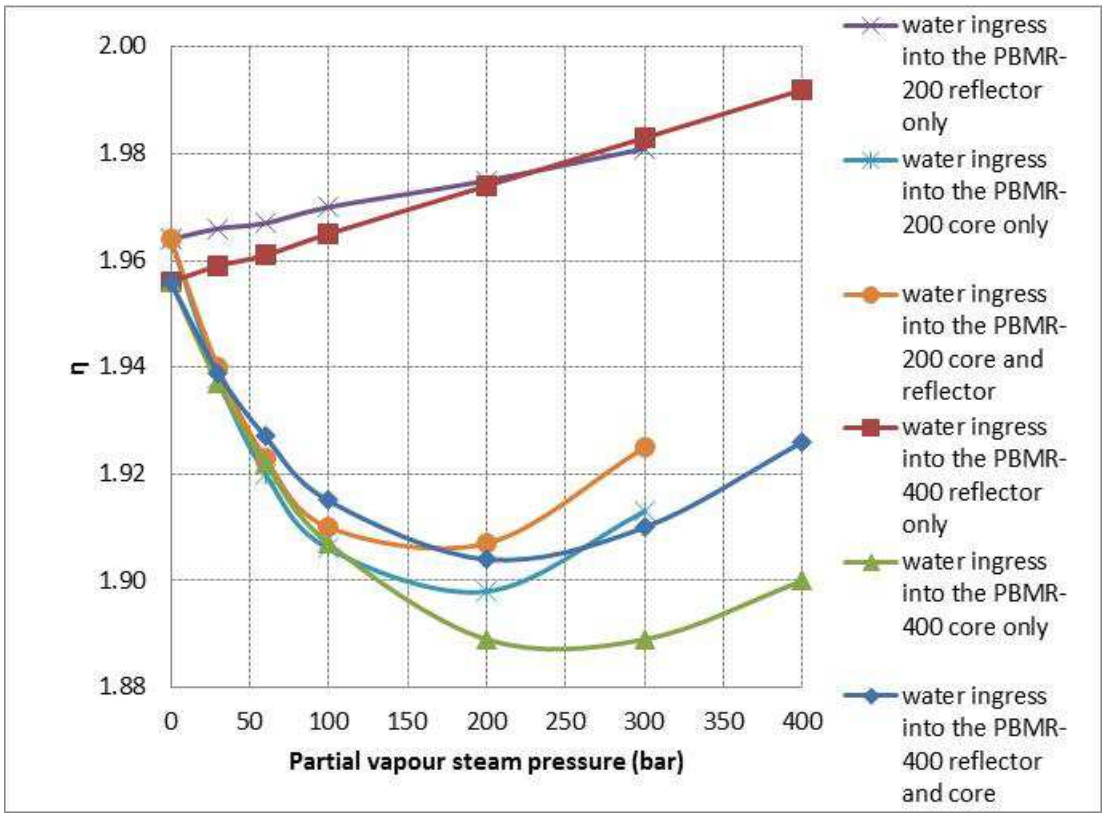

Figure 34: Distortion of η due to water ingress in the PBMR-400 and PBMR-200

It can be observed from this figure that water ingress into the PBMR-400 reflector only led to an increase in the value of η. This value increased by 0.03 for the PBMR-400 and by 0.02 for the PBMR-200. For the case of water ingress into only the core, η decreased to 1.89 for PBMR-400 and then started to increase again up to 1.90. The effects for water ingress into both the external reflector and core were similar, but less pronounced, since the decreases in η due to water ingress into the core was partly offset by increases due to ingress into the reflector. The trends for the PBMR-200 were similar, but less pronounced.

It is also observed from this figure that distortion of the value of η is inversely related to that of k_{eff}, this means that where k_{eff} was seen to decrease, the value of η increases and vice versa, as can be seen from a comparison to the case of water ingress into the reflectors in Table 6 and Table 7 above. This result is counter intuitive and unexpected: It is well known that η is high in the thermal neutron energy rage and much lower in the epithermal ranges. Therefore the expected result for water ingress into the fuel core only was that faster moderation would produce less fissions in the epithermal range and more fissions in the thermal range and would thus increase η. Therefore this strange result is referred to the list of suggested future studies.

3.2.3.1 Flux distribution results for the PBMR-400

3.2.3.1.1 Flux distribution results for the case of water ingress into the PBMR-400 reflectors only

Figure 35 below shows the radial flux distribution in the case of water ingress into the reflectors only. The fast neutron flux was taken from the energy flux group 1 with a range 0.1 MeV <E<10 MeV. The thermal neutron flux limits are 0.001 eV <E<1 eV. The scale of the fast energy group, on the right hand side of the chart, was stretched in order to magnify the difference in the fast flux before and after water ingress.

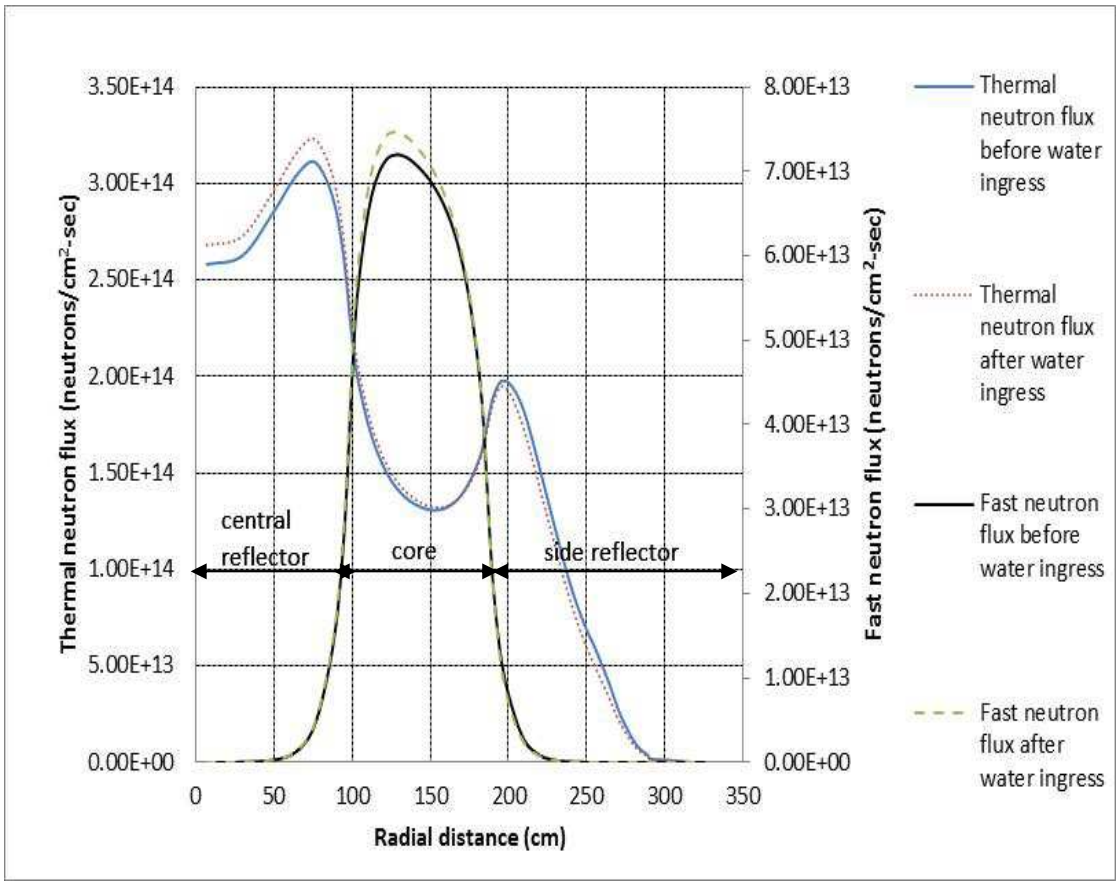

Figure 35: Flux distribution of the PBMR-400 for the case of water ingress into the reflectors only, 612 cm from the top of the core

It can be observed from this figure that water ingress resulted in a small decrease in the thermal neutron flux in the external reflector. The thermal flux, however, increased significantly in the central reflector.

Water ingress into the external reflector was expected to induce a substantially larger decrease in the fast flux in that reflector, due to faster moderation. However, the observed decrease was so small as to be almost unobservable. This was countered

by a similarly small increase in the fast flux in the central reflector. This result is counter intuitive and is thus referred to the list of suggested future studies.

When water was added into the reflectors it can be observed that the fast flux increased slightly in the core. This is also counter intuitive and is added to the referred future study.

3.2.3.1.2 Flux distribution results for the case of water ingress into the PBMR-400 core only

Figure 36 below shows the effect of water ingress into the core only on the radial neutron flux distribution.

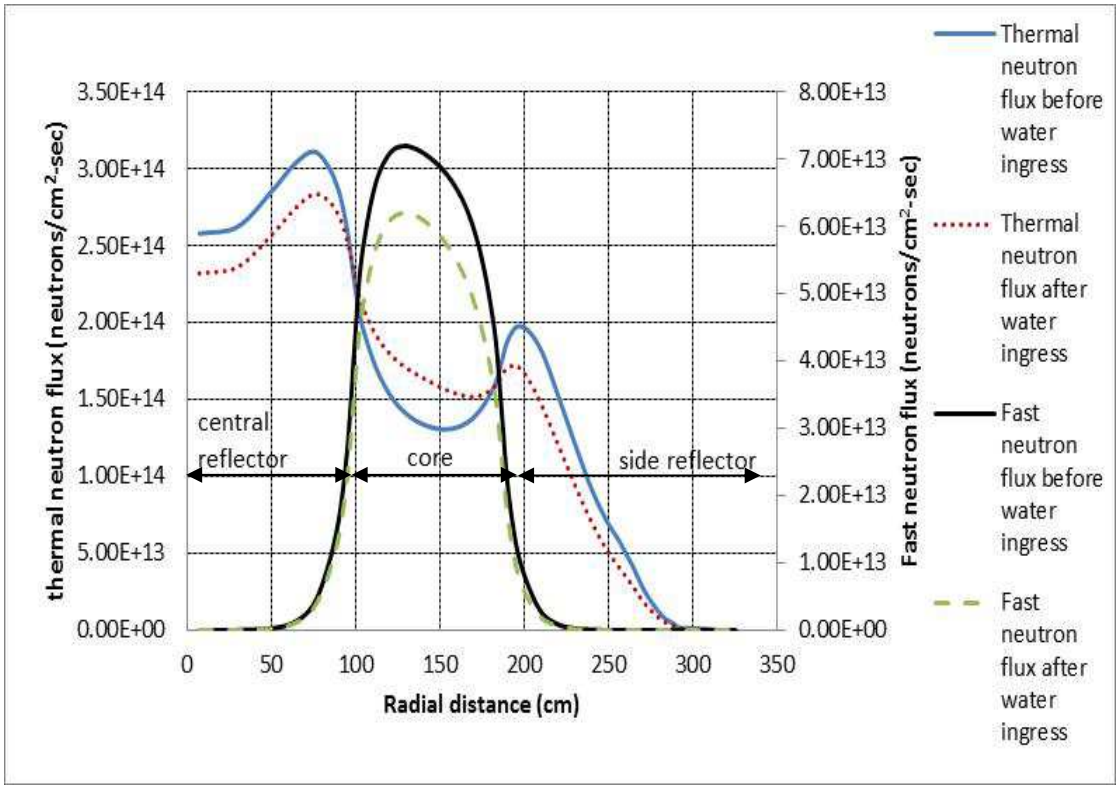

Figure 36: Flux distribution of the PBMR-400 for the case of water ingress into the core only, 612 cm from the top of the core

Water ingress into the core is observed to reduce the fast neutron flux curve, as was expected due to faster moderation. As was expected, this faster moderation led to an increased thermal flux in the fuel core. There is a substantial decrease in the thermal flux in both the central and the external reflectors, as was already explained above, i.e. due to reduced leakage of fast neutrons into the reflectors.

3.3 Comparison and validation of results

The specific factors that were postulated to influence the reactivity effect of water ingress in the two reactors were determined in the previous section for each reactor. These factors will now be compared for the two reactors and are summarised in Table 8 below.

Table 8: Summary of parameters influencing the behaviour of the reactors during the water ingress

PARAMETER	UNITS	PBMR-400 CORE AND REFLECTOR WATER INGRESS	PBMR-200 CORE AND REFLECTOR WATER INGRESS
REACTIVITY INCREASE	%	**4.05**	**4.38**
NEUTRON BALANCE:			
FRACTIONAL % NEUTRON PRODUCTION BY:			
^{235}U	%	**66.03**	**64.52**
PU-239	%	**25.89**	**27.96**
NEUTRON LOSSES IN HEAVY METALS	%	71.7	71.12
ESP. IN FISSILE ISOTOPES	%	52.53	52.45
ESP. IN PU-239	%	**14.98**	**16**
IN FISSION PRODUCTS	%	7.83	7.21
ESP. IN XE-135	%	2.58	2.51
CORE-LEAKAGE	%	**14.2**	**10.77**
FRACTIONAL ABSORPTION PER NEUTRON LOST:			
η		1.93	1.93

The main differences between the results of water ingress in the two reactors are the core leakages of 14.2% for the PBMR-400 versus 10.77% in the PBMR-200. There is also a 1.51% difference in the fractional neutron production by ^{235}U.

In (Teuchert et. al.,1992: Figure 12 curve I), a study was conducted on reactivity insertion due to water ingress of 600 kg for a moderation ratio (N_U/N_C) of a full core load of 7 g heavy metal pebbles in the HTR-Modul. These results were then used as a benchmark and compared to the PBMR-200 results as shown in Figure 37 below.

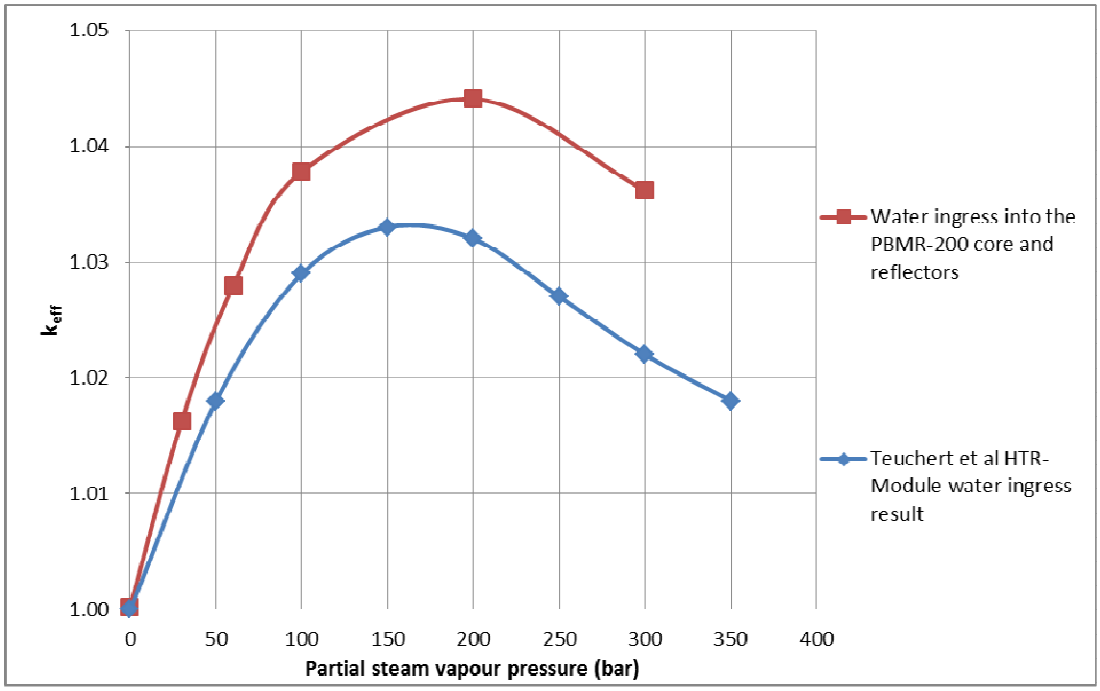

Figure 37: Comparison of water ingress event in PBMR-200 and HTR-Modul

From Table 5, the mass equivalent of the amount of water added into the core was calculated. From this table, the value that corresponds to a mass 600 kg of water can be estimated to a partial steam vapour pressure of less than 100 bar for the PBMR-200.

It can be observed from the figure above that the values of k_{eff} for the PBMR-200 values were observed to above those of HTR-Modul (Teuchert et al, 1992: Figure 12). When the partial steam vapour pressure was increased above 100 bar, the deviation became more pronounced. The maximum k_{eff} value reached for the HTR-Modul at 150 bar was approximately 1.033. For the PBMR-200, the maximum k_{eff} value of 1.044 was reached at 200 bar partial steam vapour pressure.

The PBMR-200 has the same heavy metal loading (of 7g) as the HTR-Modul but for the benchmark reactivity insertion simulation, the ^{235}U enrichment was increased from 7.8% to 8.17% (Teuchert et al, 1992: 21). This compensates for the loss in energy obtained per fuel sphere due to low heavy metal loading.

Another detail that can account for the difference in the k_{eff} values between the two reactors after water ingress could be the difference in the fuel sphere power loading which is 1.3 kW/sphere for the PBMR-200 but was increased from 1.4 to 2.1 kW/sphere in the HTR-Modul (Teuchert et al, 1992: 21).

4 Discussion of results

The simulation of the effects of water ingress on the reactivity of the PBMR-400 MW and PBMR-200 MW reactors was done and the results were compared and found to be in agreement with published literature in section 3.3 above.

It should be noted that these result were obtained using high partial steam vapour pressures of up to 300 bar for the PBMR-200 and up to 400 bar for the PBMR-400. The partial steam vapour pressures were increased until just after the peak value of k_{eff} was reached. Realistically, the primary relief systems are designed to protect the pressure vessels against overpressure. Therefore these much higher steam pressures will not be reached. During the simulations, it was found that the PBMR-400 reached its peak at a higher partial steam pressure than the PBMR-200. The expected steam pressure in the PBMR-200 should then be below 70 bar and 90 bar for the PBMR-400. The maximum realistic reactivity increase would therefore be around 3% for the PBMR-200 and 2.8% for the PBMR-400.

The following mechanism were found to drive the reactivity changes due to water ingress: core leakage, increased neutron captures in the hydrogen, graphite and fission products in the core, less captures in the resonances of ^{238}U and more fissions and less captures in the increases in η. The maximum reactivity increase for both reactors was around 4% and agrees well with the German HTR-Modul results in (Lohnert, 1992: 167).

From the lessons learnt about the mechanism that drives the changes in k_{eff} due to water ingress into respectively the reflectors and the fuel core, it follows logically that attempts to decrease the increase in k_{eff} due to water ingress into both the core and reflectors should be based upon the following strategies:

1. Increasing the volume of water ingress into the reflectors,
2. decreasing the volume of water ingress into the fuel core, and
3. decreasing the level of under-moderation in the fuel by increasing the resonance escape probability before water ingress.

Proposals for design modifications to achieve these goals are included in the proposals for future studies below.

4.1 Conclusion

The project has achieved the main objective that was set out which was to determine the details of the mechanisms and effects of water ingress on the reactivity of the PBMR-400 MW and PBMR-200 MW reactors in order to propose design changes that will mitigate these effects.

The following specific research aims were achieved:

- The characteristic behaviour of the reactors were studied for the transient event of water ingress and the impact thereof on k_{eff}, the flux distribution and power profiles.
- The difference in the mechanisms and reactivity effects of water ingress into the fuel core only, the riser tubes in the reflectors only and ingress into both the fuel core and the riser tubes in the reflectors were studied.
- The knowledge gained of these mechanisms and effects were used to propose design changes that will mitigate the reactivity increases, caused by realistic water ingress scenarios, as can be seen in the section below.
- Past results from simulations of water ingress into Pebble Bed Reactors were used to successfully validate and verify the present simulation approach and results.

4.2 Recommendations for future studies

To improve the safety of these reactors it is proposed that the following possible strategies to reduce the increases in k_{eff} during water ingress even further should be investigated in future studies:

- The ingress of water into the reflectors causes neutrons to be thermalised and absorbed by ^{1}H and graphite thereby decreasing the value of k_{eff}. If the riser channels in the external reflectors were to be increased in size or number this might allow more water ingress and more neutron thermalisation. This would help keep the reactivity increase low during a water ingress event. This effect can possibly be multiplied by inserting similar riser tubes in the central reflector of the PBMR-400. The effectiveness of such a strategy is recommended for future study.
- The central reflector further pushes the fuel spheres out towards the external reflector, thus increasing the effectiveness of the reduction of the influx of thermal neutrons back from the reflector into the core, due to water ingress into the external reflector. The effectiveness of changing the size of the central reflector should thus be studied.
- Although the geometric design of the PBMR-200, e.g. not having a central reflector, proved to be inferior with regards to mitigating the increase in k_{eff} due to water ingress into both the fuel core and external reflector, The PBMR-200 still outperformed the PBMR-400 in many aspects, due to the lower heavy metal loading of its fuel spheres, which strongly limited the reactivity increase due to water ingress into only the core. This similar measure to improve the fuel of the PBMR-400 should be investigated. Reducing the heavy metal loading, but then compensating for the loss in energy obtained per fuel sphere by increasing the enrichment of the fuel is proposed. The resulting reduction in the mass of ^{238}U per fuel sphere should lead to improved moderation, which should reduce the fraction of neutrons captured in the resonances of ^{238}U before water ingress, which should then reduce the scope for increased resonance escape probability during water ingress.
- After water ingress into the core only, fractional neutrons produced by ^{235}U substantially increased while the ^{239}Pu neutron production decreased substantially for both the PBMR-400 and PBMR-200. It is not immediately clear what drove this swing from neutron production due to fissioning of ^{239}Pu to that of ^{235}U. One possibility is the influence of the thermal fission resonance of ^{239}Pu at 0.3 eV. Therefore faster moderation, due to water ingress into the

fuel core should be investigated. This may cause more neutrons to escape this fission resonance by being thermalised before being able to produce fission in this resonance. Such a mechanism will thus reduce fissions in this ^{239}Pu fission resonance and will correspondingly increase fissions at well thermalised, i.e. lower, energies in all the fissile fuels. However, since the number density of ^{235}U is much larger than that of ^{239}Pu, such a shift to lower energies may favour fission in ^{235}U.

- The inverse relationship between η and that of k_{eff} was found to be counter - intuitive and unexpected: It is well known that η is high in the thermal neutron energy rage and much lower in the epithermal ranges. Therefore the expected result for water ingress into the fuel core only was that faster moderation would produce less fissions in the epithermal range and more fissions in the thermal range and would thus increase η. The cause for this behaviour should thus be further investigated.
- When water was added into the reflectors it can be observed that the fast flux increased slightly in the core. The reason for this unexpected behaviour should also be investigated.

5 References

DOE. 2011, Department of Energy RSA Homepage, http://www.energy.gov.za/files/IRP: Integrated Resource Plan 2010-2030, Rev 2, 25 March 2011. Date accessed: 11 July 2012.

Geringer W. 2010. The influence of the number of fuel passes through a pebble bed core on the coupled neutronics / thermal-hydraulics characteristics, November 2010. Masters mini-dissertation. North-West University, South Africa.

Greyvenstein R. 2008. Correia M., Kriel W., South Africa's opportunity to maximise the role of nuclear power in a global hydrogen economy, Nuclear Engineering and Design 238 (2008) 3031–3040.

Nuclear Regulatory Commission. 2010. HTGR Technology Course for the Nuclear Regulatory Commission 2010, Module 6a, Pebble Bed HTGR Core Design Description, 24-27 May 2010.

Hartnady C. 2010. South Africa's diminishing coal reserves. http://www.sajs.co.za South African Journal of Science 2010; 106(9/10), Article #369, 5 pages. DOI: 10.4102/sajs.v106i9/10.369. Date accessed: 04 March 2013.

Kugeler K., Stulgies A. and Epping Ch. 1988. Aerosol Formation During Water Ingress Into the Core of a Pebble Bed High-Temperature Reactor, Aerosol Science and Technology 9: 3, 177 — 187, Duisburg, Germany, 01 January 1988.

Lamarsh J. and Baratta A. 2001. Introduction to Nuclear Engineering, Third edition, Prentice-Hall, Inc., New Jersey.

Lohnert G.H. 1992. The consequences of water ingress into the primary circuit of an HTR-Modul – From design basis accident to hypothetical postulates, Nuclear Engineering and Design134 (1992) 159-176, North Holland.

Lohnert G.H. 1990. Technical Design Features and essential safety-related properties of the HTR-Modul, Nuclear Engineering and Design129 (1990) 259-275, North Holland.

Matzner D. 2004. PBMR Project Status and the Way Ahead, 2nd International Topical Meeting on High Temperature Reactor Technology, Beijing, China, September 22-24 2004.

McKune C. 2010. Pebble bed modular reactor demonstration plant is funded but not constructed. S Afr J Sci. 2010, Art.#287, DOI:10.4102/SAJS.V106I5/6.287.

Moormann R. 2002. Fission Product Behaviour: Release from fuel, transport, deposition, remobilsation and retention under normal and accident conditions, HTR/ECS 2002, Project European Spallation Source, Forschungszentrum Jülich.

Moormann, R. 2008. A Safety Re-evaluation of the AVR Pebble Bed Reactor Operation and Its Consequences for Future HTR Concepts. Forschungszentrum, Zentralbibliothek, 2008.

Moormann R. 2009. AVR prototype pebble bed reactor: a safety re-evaluation of its operation and consequences for future reactor, Nuclear Engineering Journal, Germany, 2009.

Mulder E. et al. 2010. Thorium and Uranium Fuel Cycle Symbiosis in a Pebble Bed High Temperature Reactor, proceedings of HTR 2010, Prague.

Mulder E. 2010. Theoretical Description of VSOP, Pebble Bed Reactor Design (NUCI886): M.Eng./M.Sc. Lecture Notes, 2010.

Nuclear Regulatory Commission (NRC) 2010, Module 6a, Pebble Bed HTGR Core Design Description, HTGR Technology Course for the Nuclear Regulatory Commission, May 24 – 27, 2010.

Nuclear Energy Corporation of South Africa (NECSA). 2012. Nuclear Power in South Africa, http://www.necsa.co.za/Portals/1/Documents/b8171927-6bbe-4a32-a45fe4176fcfa7c5.pdf, updated August 2012. Date accessed 17 April 2013].

Reitsma, F. 2004. The Pebble Bed Modular Reactor Layout and Neutronics Design of The Equilibrium Cycle. In: Proc. PHYSOR2004, Chicago, USA, 25–29 April 2004.

Reitsma F. 2011. The Pebble Bed Modular Reactor Design and Technology Features, Advanced Nuclear Reactor Technology for Near Term Deployment, IAEA Inter-regional Workshop 4-8 July 2011.

Reitsma, F. 2012. Reactivity considerations for the on-line refuelling of a pebble bed modular reactor—illustrating safety for the most reactive core fuel load. Nuclear Engineering and Design 251 (2012) 18– 29.

Rütten H.J. et al. 2007, V. S. O. P. (99/05) - Computer Code System for Reactor Physics and Fuel Cycle Simulation, Release 2, Jül-4189.

RSA. 2012. SA Yearbook 2011/12, 2012, 19th edition, Government Communication and Information System (GCIS), Pretoria, SA, pg 409-421, April 2012.

Serfontein D.E. 2011. Deep Burn Strategy for the Optimized Incineration of Reactor Waste Plutonium in Pebble Bed High Temperature Gas-Cooled Reactors, PhD thesis, North-West University, South Africa.

Steinwarz, W., Yuanhui, X. 1990. Status of design of the HTR-test module China. Nuclear Engineering and Design 121 (2), 317–324.

Teuchert E. et al. 1987. Distribution of the Decay Heat in Various Modul HTRs and Influence on Peak Fuel Temperatures, Energy Conversion Engineering Conference, Philadelphia, PA 10-14 August 1987.

Teuchert E. et al. 1992. Rechnerische Darstellung des HTR-Modul Reaktors, Jül-2618, Jülich Report, May 1992.

Theenhaus R. and Storch S. 1990. The AVR-High Temperature Reactor – Operating Experience, Storage and final Disposal of Spent Fuel Elements, Research Centre Jülich GmbH, Federal Republic of Germany, 1990.

Thomas S. 2011. The Pebble Bed Modular Reactor: An obituary, Energy Policy 39 (2011) 2431–2440, Elsevier Ltd.

Venter P.J. 2009. PBMR-200 Summary Technical Description-110652 Rev 1.

Wu Z., Lin D., Zhong D. 2002. The design features of the HTR-10, Institute of Nuclear Energy, Nuclear Engineering and Design 218 (2002) 25–32, Elsevier Science B.V.

Zheng Y. et al. 2010. Water-ingress analysis for the 200 MWe pebble-bed modular high temperature gas-cooled reactor. Institute of Nuclear and New Energy Technology, Tsinghua University, Beijing 100084, China. Nuclear Engineering and Design *240* (2010) pp. 3095–3107.

Zuying G., Lei S. 2002. Thermal hydraulic transient analysis of the HTR-10, Institute of Nuclear Energy Technology, Nuclear Engineering and Design 218 (2002) 65–80.

Zuying G., Chuyun W., Baoyan L. 1993. Transient Analysis of Water Ingress into the HTR-10 High Temperature Gas Cooled Reactor, Insitute of Nuclear Energy Technology, Tshinghua University, Beijing, China. pg 92-96.